To the Graduate Council:

I am submitting herewith a thesis written by Franz-Josef Kahlen entitled "The development of a laser reflectometer diagnostic technique for laser keyhole welding studies of stainless steel SS 304". I have examined the final copy of this thesis for form and content and recommend that it be accepted in partial fulfillment of the requirements for the degree of Master of Science, with a major in Aerospace Engineering.

T. Dwayne McCay, Major Professor

We have read this thesis
and recommend its acceptance:

Accepted for the Council:

Associate Vice Chancellor
and Dean of the Graduate
School

Statement of Permission to use

In presenting this thesis in partial fulfillment of the requirements for a Master's degree at The University of Tennessee, Knoxville, I agree that the library shall make it available to borrowers under the rules of the library. Brief quotations from this thesis are allowable without special permission, provided that accurate acknowledgement of the source is made.

Permission for extensive quotation from or reproduction of this thesis may be granted by my major professor, or in his absence, by the head of the Interlibrary Services when, in the opinion of either, the proposed use of the material is for scholarly purposes. Any copying or use of the material in this thesis for financial gain shall not be allowed without my written permission.

Signature Franz-Josef Uahle

Date April 27, 1994

The development of a laser reflectometer diagnostic technique for laser keyhole welding studies of stainless steel SS 304

A Thesis

Presented for the

Master of Science

Degree

The University of Tennessee, Knoxville

Franz-Josef Kahlen

May 1994

Dedication

This thesis is dedicated to my parents

Heinz and Sophia Kahlen

who have supported the education of their

children wherever possible.

Acknowledgments

I would like to thank my major professor, Dr. T. Dwayne McCay, for giving me the opportunity to continue my work with laser diagnostics. I also thank him for his guidance during my study here at UTSI and the fair attitude he shows towards students. I would also like to acknowledge the assistance and the feedback I received from the other members of my committee, Dr. Mary Helen McCay and Dr. Roger Crawford. I want to mention the comments I received from Dr. Vakili and Dr. Smith here at UTSI. Getting started as well as performing my experiment would not have been so smooth without the continued help of Cindy McKowen and Carl Schou.

Special thanks go to my fiance Miho Mizuguchi for her encouragement. She distracted me from my work whenever I did not see the forest for the trees and helped me to take a wider perspective.

Among those who helped me get where I am are also Prof. Rudolf Schulten, Prof. Hans Bonka, and Prof. Klaus-Dieter Broichhausen from the Rheinisch-Westfälisch Technische Hochschule Aachen. Thank you very much to all of you.

Abstract

It is generally understood that in deep penetration laser welding, a keyhole is formed in the weld pool through which the laser energy is transported far inside the workpiece. However, no detailed, universally accepted physical explanations are available.

To provide further insight into the phenomena, a diagnostic technique called a laser reflectometer for monitoring the surface behavior of a sample and the keyhole during CO_2 laser welding was developed. A low power Argon probe laser beam was focused on a weld pool created in stainless steel SS 304 by a RS3000 CO_2 laser operated in single pulse mode at peak powers from 500 W to 2500 W.

The laser reflectometer data allow to distinguish between reflections from a conduction limited weld and a deep penetration weld. The technique was applied to monitor the weld pool on the upper sample surface as well as the point of penetration on the lower surface. Information about the phase transition time of the material on the upper surface and the penetration time of the laser energy through the sample could be gained. Variations in the probe beam reflected intensity from two different sample thicknesses were detected, identifying the surface waves and providing information about their frequency and velocity. The results identify strong oscillations of the weld pool surface during the welding process around its resonance frequency of 200 Hz to 350 Hz and around 800 Hz. The surface wave velocity was calculated as 0.4 m/s. The amplitude of these waves is estimated as 40 μm.

Table of Contents

List of Tables

List of Figures

Nomenclature

c_p	[J/(kg*K)]	specific heat (at constant pressure)
DC		Direct Current (off-set for the FFT)
FFT		Fast Fourier Transformation
Fr		Froude Number
g	[m/s^2]	gravitational constant
HeNe		Helium Neon
HgCdTe		Mercury-Cadmium-Telluride Detector
Hz	[1/s]	Hertz
I	[W/cm^2]	Intensity of the laser beam
k	[W/(m*K)]	thermal conductivity
L_f	[J/kg]	latent heat of fusion
L_v	[J/kg]	latent heat of vaporization
l	[m]	length scale
m		meter
NDF		Neutral Density Filter
ND		Neutral Density
PMT		Photomultiplier Tube
PWM		Pulse Width Modulation

RF		Radio Frequency
s		seconds
t	[s]	Time
T	[K]	Temperature
V	[m/s]	Velocity
W		Watt

Greek letters

α	coefficient of laser energy absorption of the material
μ	viscosity
ρ	density
γ	coefficient of surface tension
$\varkappa$	thermal diffusivity

Indices for time and temperature

m	melting
v	vaporization

1 Introduction

When using industrial lasers for a welding process, most operators judge by previous experience how much power is needed for the desired speed. This can often result in full penetration welding, in cutting, or in partial penetration welding. The efficiency of the welding process would be maximized if enough power were supplied to achieve full penetration of the weld without overpenetration. In order to produce such a fully penetrated quality weld, the energy transfer into the lower regions of the material must be enhanced while keeping the lateral energy transfer at a minimum, thus providing a small heat affected zone. It is general understanding that a cavity ("keyhole") is formed in the weld pool during deep penetration laser welding through which the energy is deposited inside the material; however, universally accepted explanations of the details of this phenomena are not available.

To obtain a better understanding of the keyhole and surface behavior during the welding sequence, a diagnostic technique capable of monitoring the weld pool during processing was developed. For this purpose, a second, high intensity light source was focused at either the top or bottom surface of the weld pool and reflections were detected by a Photomultiplier Tube (PMT). This thesis addresses the development of this technique called "laser reflectometer" and provides interpretations of the acquired data. A detailed description of this diagnostic technique will be given in chapter 3 "Experimental Approach".

Parameters to be varied were the supplied CO_2 laser peak power and the sample thickness. Different peak powers were achieved by alterations of the RF-power. Although not the main purpose of this investigation, it is also possible to apply the technique to determine if the laser beam has fully penetrated the material.

2 Background

2.1 Introduction

Several diagnostic techniques have been used to optically investigate the behavior of the weld pool under the influence of a heat source. The following literature search summarizes these techniques and outlines their results.

During the welding process the weld pool will be exposed to temporarily varying source functions like jitter in the laser processing speed and shield gas leakages. Very few attempts have been made so far to analyze the resulting unsteady weld pool behavior theoretically and to model the dynamics of a pool of molten metal. The results of these investigations will also be presented.

2.2 Formation of a keyhole in the weld pool during laser welding [8]

When a metal surface is exposed to a sufficiently high energy intensity, the material will heat up until its melting temperature is exceeded and a molten weld pool forms. At the region of the pool center, the vaporization temperature is also eventually exceeded. The vaporized material leaves a depression with a very large radius of

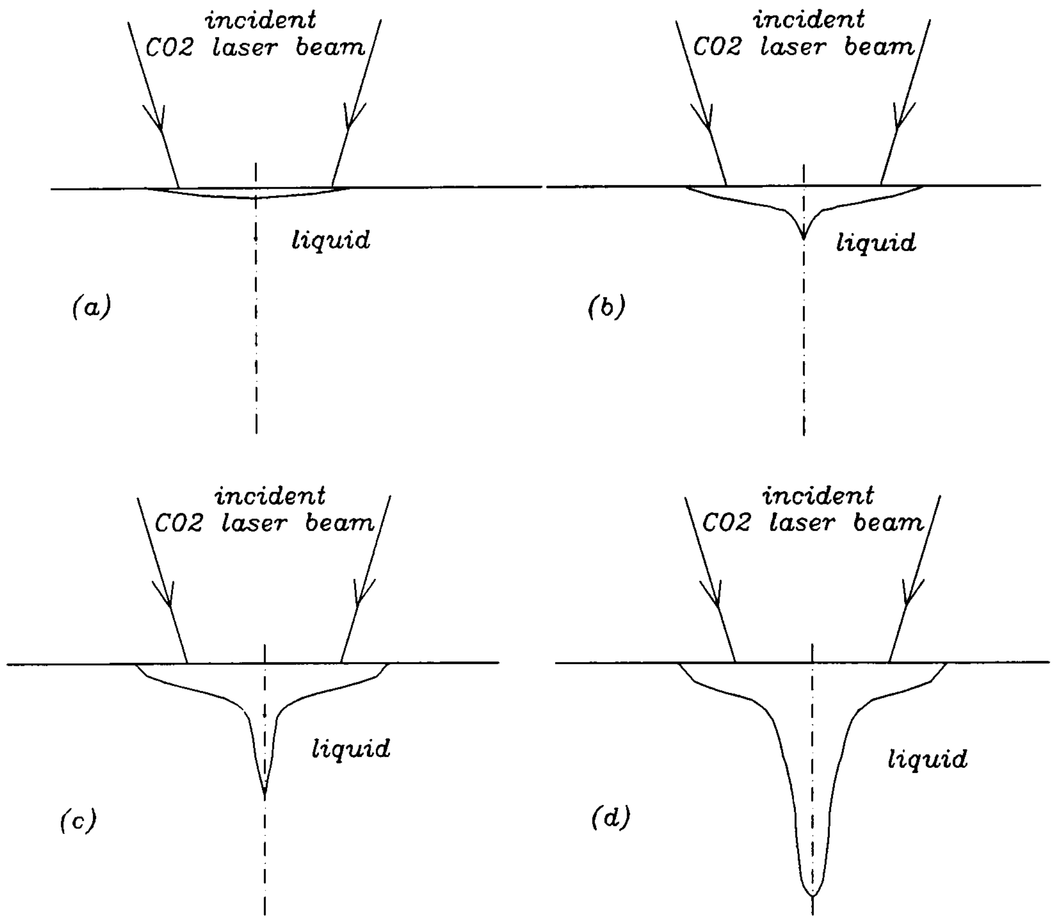

Figure 2.1 Keyhole formation. The figures show the development of the liquid-vapor interface beginning with the formation of an overall depression of the weld pool (a) where the vapor phase occupies the region betweeen the liquid-vapor interface and the sample surface. The radius of the depression grows under the continued presence of the CO_2 laser beam and forms a hole at the point where the material is exposed to the highest intensity in the laser beam (b). This hole continues to grow (c) up to the point where the vapor pressure can be balanced by the surface tension forces (d).

curvature in the weld pool. In this initial stage, the vaporization pressure on the molten surface is much larger than the pressure due to surface tension since the latter one is inversely proportional to the radius of curvature of the depression (Laplace's formula). As a result, the vaporization pressure will deepen (and to a lesser extent widen) the depression up to the point where the vaporization pressure is balanced by the surface tension (see Figure 2.1, a - d). Thereby, a cavity ("keyhole") is formed in the weld pool which may extend deep into the workpiece once it is fully established (see Figure 2.2 for the geometry of the weld pool).

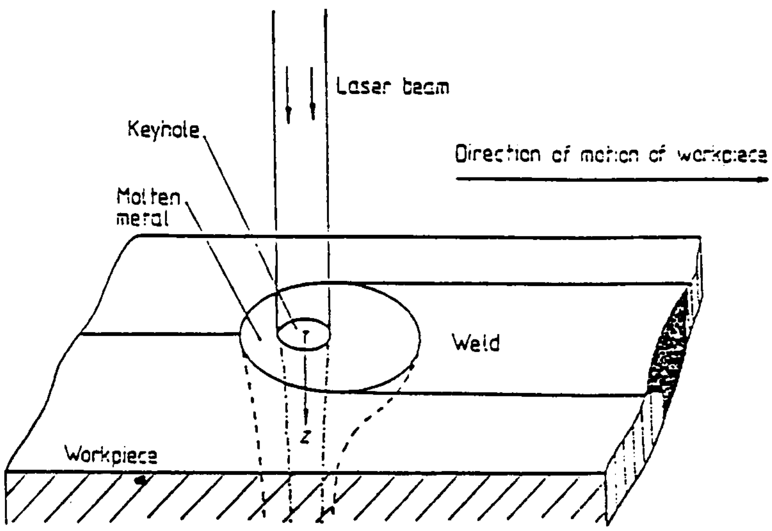

Figure 2.2 Geometry of the CO_2 laser beam relative to the workpiece in laser keyhole welding [picture taken from [7] Dowden, J.; Kapadia, P.; Postacioglu, N.; *An analysis of the laser-plasma interaction in laser keyhole welding*; J. of Physics D, Applied Physics, Vol. 22, pp. 741 - 749]

2.3 Observations of the weld pool

Observing the interaction of the laser beam with a metal material is difficult. The interaction process occurs rapidly, a very bright surface plasma forms close to the keyhole, and the material is opaque. Hence for metal welding, optical inspection of the welding process is limited to monitoring the surfaces of the sample. However, for transparent materials such as glass and some plastics, a visual examination of the process occurring inside the material is possible.

Arata [2 - 5] has used several different diagnostic techniques to monitor the behavior of the weld pool inside transparent materials. Experimental investigations in glass have recorded the formation of a cavity in the weld pool for both stationary and moving samples [2]; some flow structures could also be resolved. He recorded the behavior of the weld pool in the sample; however, pictures taken at 1000 frames per second could not resolve flow patterns in some regions of the liquid material.

Two other methods applicable to observe the weld pool behavior were suggested by Arata [4]. For one method, heat proof glass was put next to the investigated material. The welding took place inside the material at the glass-material boundary. Another method, called "beam-hole X-ray" [5], involved observing hard x-rays transmitted through the weld region. Both methods showed the contours of the weld region but they lacked features about the keyhole and flow structures making them acceptable only for preliminary studies.

2.4 Analytical investigation of unsteady keyhole behavior

Recently, Kroos, Gratzke, and Simon [11] considered the case when an established keyhole changes its shape during the welding process. This assumption deviates from previous cases considering keyholes of fixed shape and since one always has to deal with realities such as power fluctuations, shield gas leakages, and work table jitter, this condition is much more realistic. A linear stability analysis of the established keyhole predicted oscillations of the keyhole walls in the range of 500 Hertz to 700 Hertz.

2.5 Summary:

Theoretical investigations of the unsteady behavior of the weld pool in deep penetration laser welding have just begun. They predict oscillations of the keyhole of several hundred Hertz.

Different diagnostic techniques have been proposed and used to investigate the behavior of the weld pool during the welding sequence. However, the results lack the desired temporal resolution to provide information about phenomena like e. g. the keyhole formation and the surface wave characteristics. The reflectometer technique used in this research is capable of detecting keyhole oscillations as well as rapidly changing surface structures of the weld pool. It is limited in terms of the temporal resolution only by the sampling frequency of the data acquisition system. Thus, this technique and the information gained by applying it will be of value in understanding the weld pool behavior.

3 Experimental Approach

3.1 Introduction

The experimental equipment for the laser reflectometer technique consists of an Argon laser, the optical components required for the delivery of its beam to the sample surface and for its detection, and the data acquisition system. Each component will be introduced individually and a list of all equipment used is included as Appendix B. All runs were performed twice; the general conditions for these runs are listed in Table 3.1. The descriptions include a summary of sources of noise and vibration in the laser vicinity followed by a general performance critique of the CO_2 laser.

Table 3.1 Material and laser conditions investigated

material	Stainless Steel SS304
shield gas	Helium (coaxial)
pulse length [ms]	30
PWM [%]	100
peak power levels [W]	500, 1000, 1500, 2000, 2500
sample dimensions [mm]	25.4 x 25.4 x 1 and 25.4 x 25.4 x 3

3.2 Argon laser and delivery optics

A 3 W Argon laser probe beam (operating at 514.5 nm) was used as the high-intensity light source for the reflectometer. The beam was focused to a spot size of 20 μm at the weld pool using a 10 cm focal length lens. For the alignment, spot welds were created on the sample and the Argon laser beam was positioned at a distance of about 350 μm from the center of the spot weld. Then, the sample was translated about one centimeter so that the Argon laser beam hit an unprocessed surface.

The diagnostic technique allows to monitor the weld pool on the upper surface as well as the point of penetration of the spot weld on the lower surface. Each surface was monitored separately. In the case of the upper surface, the probe laser beam was aimed at the weld region (Figure 3.1 a) at an angle of 40 degrees with respect to the CO_2 laser beam; this angle being determined by the shield gas nozzle. On the lower surface, the point of penetration of the spot weld was observed (Figure 3.1 b). This surface was monitored at an angle of ten degrees with respect to the CO_2 laser beam; the angle determined by the mounting equipment for the focusing lens.

To avoid scattering of the incident Argon laser beam due to the surface structure of the sample, the samples were polished. Comparing the signals recorded with an oscilloscope for polished and unpolished stainless steel SS 304, the data differed only in the amplitude of the Argon laser beam reflected from the unwelded surface. The signal recorded during and after the welding process showed no difference; but, since more Argon laser light was reflected from the polished surface, the initial signal from the

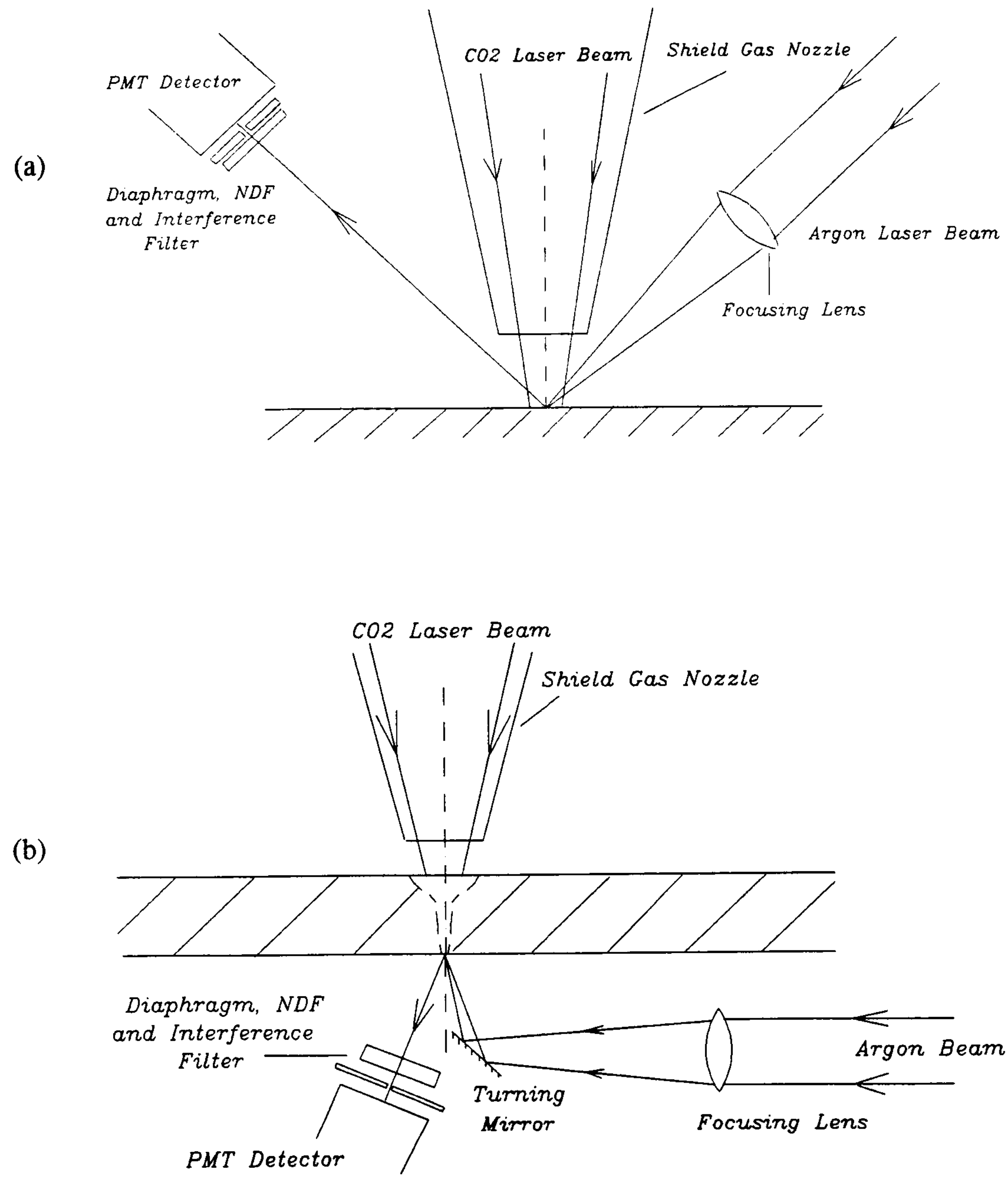

Figure 3.1 Alignment scheme for (a) monitoring the weld pool on the upper sample surface and (b) monitoring the penetration point on the lower sample surface

photomultiplier tube (PMT signal) was higher. Since no other differences were found, the data was recorded for samples of polished stainless steel SS 304. It was also easier to align the PMT when the Argon laser beam was reflected from a polished surface.

3.3 Detection optics for the Argon laser beam

The reflections of the Argon laser beam from the weld region were detected with a Hamamatsu R212 photomultiplier tube (PMT) at a distance from the weld pool of 25 cm. The sensitive area of the PMT had an opening of 1 mm. To reduce the effect of plasma induced radiation and stray light (e. g. room light), an interference filter centered at 514.5 nm with a bandwidth of 10 nm was placed in front of the opening of the PMT. The room lights were turned off during the experiments to avoid contamination of the PMT signal with frequencies of 60 Hz and its harmonics. Saturation of the PMT was avoided by neutral density filters (NDF, ND 4 and ND 5) placed in the path of the reflected Argon laser beam.

Test runs with and without sample illumination by the Argon laser beam were performed to ensure that the illumination caused by the plasma above the weld pool was insignificant compared to the Argon laser beam reflection. Without the Argon laser on, no signals were recorded by the PMT during a run. For the case with the Argon laser beam illuminating the weld region, the data showed the temporal changes of the Argon probe beam signal for all welding conditions.

3.4 Sample mount and configuration

The Argon laser, the delivery optics for the Argon laser beam, the PMT, and the sample were mounted on a table detached from the workstation. This was necessary in order to reduce mechanical noise transmitted into the optical set-up (see chapter 3.6).

The sample was clamped to the mounting equipment so that it formed a cantilever of approximately 15 mm length. This cantilever's resonance frequency can be calculated [6] from

$$\omega = \sqrt{\frac{3EI}{0.23ml^3}} \tag{3.1}$$

where E is Young's modulus, I is the moment of inertia of the sample, m is its mass, and l is the length of the cantilever. Taking material properties as listed in Appendix C, a resonance frequency of the clamped sample of about 24 kHz was calculated.

3.5 Data acquisition system

The PMT output is a current signal and is changed into a voltage signal in order to be recorded. A resistor of 50 kΩ was used as a terminating impedance. The size of the resistor was chosen in order to keep the RC-time constant of the resistor and the coaxial cable small. Multiplying the resistance with a maximum current in the PMT [10] gives a maximum output voltage of the PMT to about 200 mV.

The CO_2 laser pulse, the drive current for the RF tube, and the PMT signal were recorded simultaneously with a sampling frequency of 333 kHz.

3.6 Sources of noise and vibration in the laser vicinity

Preliminary investigations at the CLA have shown that the alignment of the laser reflectometer is susceptible to mechanical vibrations originating from the workstation and other surrounding equipment. These vibrations can be introduced by the two chillers that operate adjacent to the laser, the workstation, the CO_2 laser itself, and by a vacuum pump that operates occasionally; the same sources can also generate electrical noise on the line for the high-voltage power supply of the PMT. As described in chapter 3.4, all equipment was mounted to a separate table to minimize the transmission of these vibrations.

3.7 CO_2 laser

A Rofin-Sinar RS3000 CO_2 laser delivering peak powers from 500 W to 2500 W to the sample surface was used for the experiments. The CO_2 laser beam was focused to a spot size of approximately 250 μm at the sample surface using a parabolic copper mirror of 150 mm focal length. The laser was operated in single pulse regime with a pulse duration of 30 ms creating bead-on-plate spot welds in Stainless Steel SS 304. When the peak power was reduced to 500 W, conduction limited spot welds were created on the sample surface. Higher power levels created deep penetration welds. For the fully penetrated spot welds, it was verified that the lower surface of the keyhole opened during the weld sequence. For this purpose, paper was placed about 1 cm underneath the sample. This paper began to burn during the weld pulse.

The laser was calibrated with a Scientech calorimeter (Appendix B) for these power levels, tuned (by optimizing the standing wave ratio delivered from the RF-unit), and the focal distance was measured and verified. To minimize the time between "warming up" the CO_2 laser and the actual start of the CNC-program, a "warm-up" phase of 15 seconds was programmed into the CNC-program. Helium at a coaxial flow rate of 4 gallons/minute was used as the shield gas to reduce the effect of the near-surface plasma brightness.

3.8 Verification of RF-power variations

At The University of Tennessee Space Institute's Center for Laser Applications, the investigation presented here was the first one to use RF-power variations systematically in order to obtain different peak output powers. Therefore, it was necessary to verify that the intensity distribution in the resulting CO_2 laser beam (i. e. its mode) was not affected and that this method provided repeatable drive current signals from the RF-unit to the laser head.

For this purpose, mode prints of the CO_2 laser beam were taken in plexiglass to see if any changes developed. The 45° turning mirror was removed and the mode prints were taken at a distance from the CO_2 laser equal to the length of the optical beam path (5 m) from the laser head through the beam delivery optics to the sample. The RF-power was varied over the range from 420 to the level of ignition (180) while the CO_2 laser was run in PWM mode at 100 %. A visual inspection of these prints (profile, diameter) did not reveal a change in the shape of the mode.

The drive current from the RF-unit was recorded for all runs to verify that the level of the drive current signal was repeatable for the same output power levels. The changes in the drive current levels were repeatedly proportional to the resulting changes in the power levels in the CO_2 laser beam. The drive current signal showed the 5 kHz PWM modulation during the laser pulse, the leading edge spike in the beginning of each 200 μs pulse width, and a contamination by the 60 Hz line frequency. This 60 Hz component is superimposed on the drive signal at the point where the signal is monitored. It is *only* present at this point and not part of the drive current entering the laser head.

Based on these results, it was concluded that the RF-power variations above the 500 W level provided a reliable method of altering the peak power of the CO_2 laser beam.

3.9 Description of the CO_2 laser conditions

Many spot welds on the upper surface of the sample had an elliptical shape that was probably caused by an asymmetric intensity distribution in the CO_2 laser beam. Since it was checked that the beam delivered from the laser had a symmetric intensity distribution it must be concluded that distortions were introduced in the system of the beam delivery optics (Figure 3.2). In this system, sources for these distortions can be astigmatism due to misalignment of the parabolic mirror [1] and damages of the coating of the optical components.

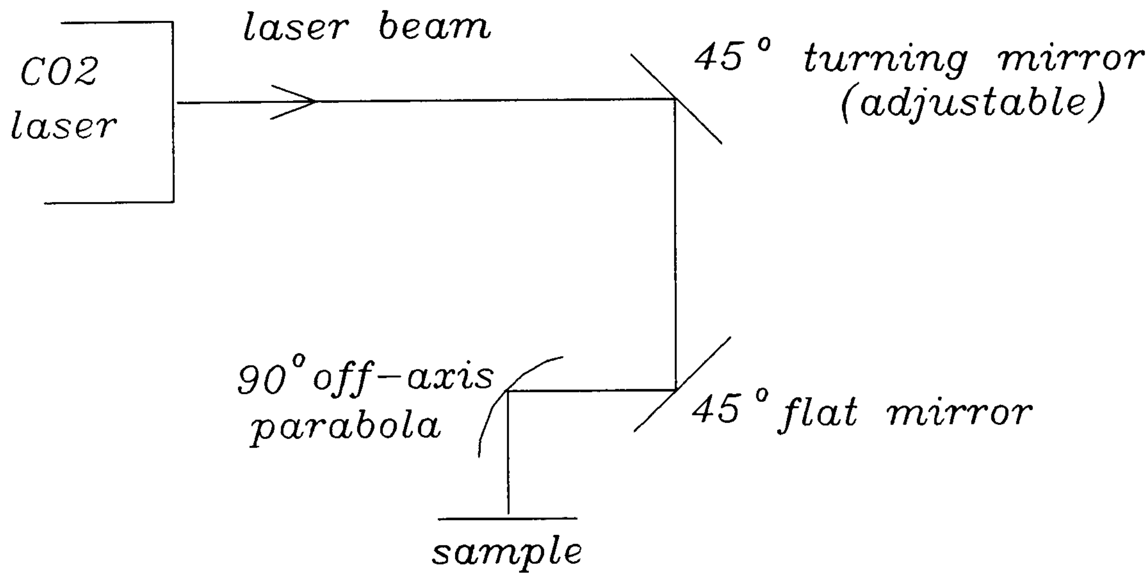

Figure 3.2 Schematic of the CO_2 laser beam path from the laser head to the sample surface and the components involved.

During the operation of the CO_2 laser, it could be seen that the HeNe alignment beam moves over the ZnSe-window mounted above the 45° flat mirror and the 90° degree off-axis parabolic mirror. It was verified that the CO_2 laser beam and the HeNe laser beam were aligned together at this point; therefore, the CO_2 laser beam moves along the same track as the HeNe laser beam. The movement of this HeNe laser beam can be observed by eye within a time period of one hour. In the morning, the beam moves away from the CO_2 laser and in the afternoon, it moves back. Due to this motion, the angle of incidence of the CO_2 laser beam with respect to the surface normal of the ZnSe-window changes over the course of the day. As a result, the CO_2 laser beam will have an angle of incidence with respect to the optical axis of the off-axis parabola; it has also been shown experimentally that the HeNe beam hit the off-axis parabola by as much as 1 cm from its center. Consequently, the alignment of the beam was checked several times during the day. The HeNe beam could not easily be aimed at the center of the ZnSe-window and the off-axis parabola simultaneously. By adjusting the 45° turning mirror the HeNe beam was pointed close to the centers of the ZnSe window and the off-axis parabolic mirror.

In addition, the coating on the surface of the off-axis parabola is severely damaged. The effect can be visualized by taking a print of the unfocused beam in plexiglass about 20 cm beneath the nozzle exit plane. Due to this damage, the intensity distribution in the CO_2 laser beam is affected. This adds to the problem introduced by the astigmatism though it is less strong.

To verify that the sample was placed at the focal distance of the parabolic mirror, the distance from a mark on the mount of the delivery optics was varied from 116 mm to 118 mm where the focal distance from this mark would be 117.5 mm. Spots were taken in increments of 0.5 mm with about 30 seconds between each spot. The spot taken at 117.5 mm distance was the most circular one; also, the other spots had an elliptical shape with their major axis pointing in varying directions indicating rotating spots.

4 Results and Discussion

4.1 Introduction

Before entering the discussion of the results, it will be helpful to introduce all features of the PMT signal first. Since some characteristics repeat in the PMT signals, it will be divided into three segments.

It is the main intention to describe the PMT signal and to analyze the information contained in it. If possible, the information gained by using the laser reflectometer will be compared to information already available. Thereby, the data gained from the laser reflectometer will be confirmed, the usefulness of the new technique will be demonstrated, and the new information will gain a high credibility.

The reader is reminded that a PMT produces a negative signal proportional to the intensity of the light received, hence, as the light intensity increases, the PMT signal increases in a negative direction.

4.2 Features of the PMT signal

The PMT signal shows a different behavior for a conduction limited and a deep penetration weld. For incident CO_2 laser powers of 500 W, a conduction limited weld was created on the sample surface but higher power levels resulted in the formation of a keyhole in the weld pool. The behavior of the PMT signal is schematically shown in Figure 4.1 (a) for deep penetration welds and in Figure 4.1 (b) for conduction limited welds. From its initial level (before the CO_2 laser pulse) the signal transitions in less than two milliseconds to a lower level (baseline level) during the pulse. During the pulse, the signal remains at this lower level with (strong) oscillations sometimes appearing in the PMT signal. After the end of the CO_2 laser pulse, the PMT signal shows other oscillations which start shortly after the pulse ends. Since all PMT data can be described by this pattern (conduction limited welds and deep penetration welds), the signal will be divided into the following three segments for discussion:

* Segment I: transition period in the beginning of the pulse before the PMT signal reaches its baseline level
* Segment II: during the CO_2 laser pulse, from the time when the PMT signal reaches its baseline level to the end of the pulse
* Segment III: after the pulse

As typical examples of the PMT signal, the following results are included:

(a)

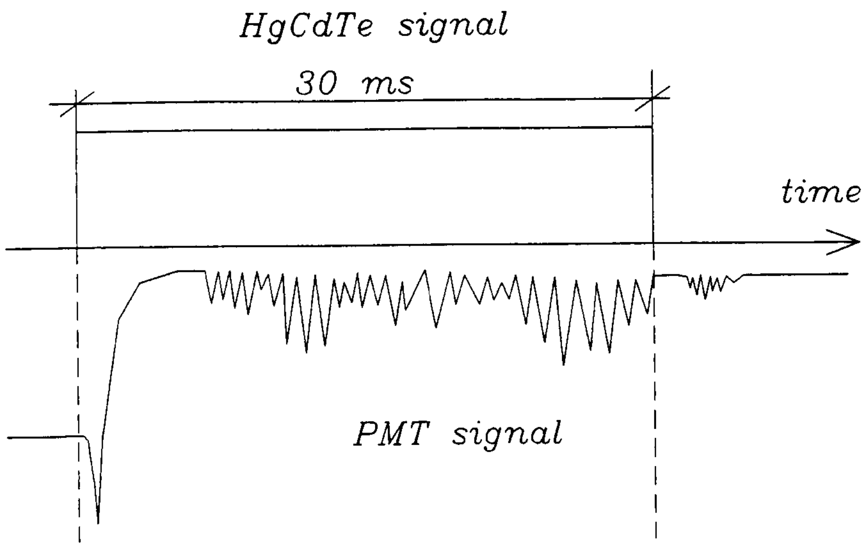

(b)

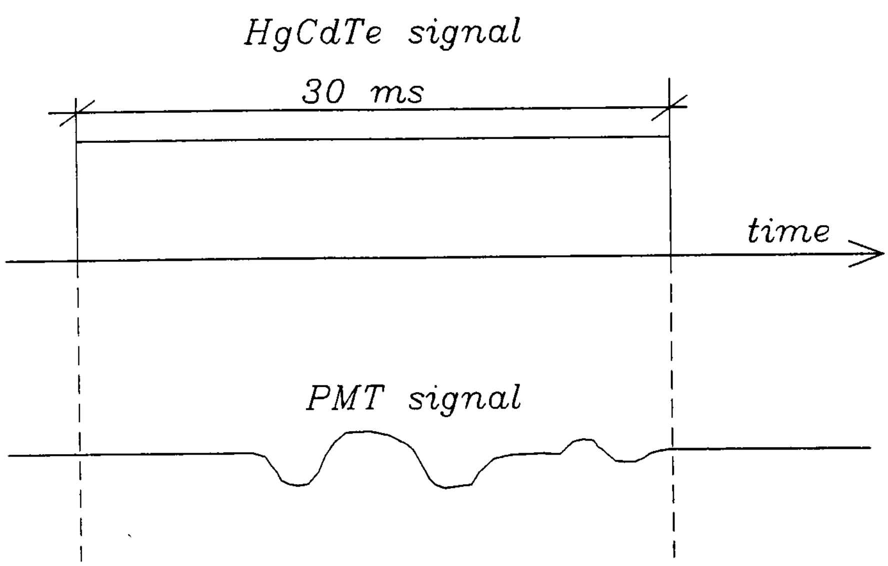

Figure 4.1 Schematical behavior of the PMT signal for (a) a deep penetration weld and (b) a conduction limited weld

* 1500 W/1 mm is shown in Figure 4.2 as an example of the PMT signal from a deep penetration weld. The figure includes an overview of the whole sampling period (Figure 4.2 (a)), an expanded plot of the HgCdTe and the PMT signal during (Figure 4.2 (b) and after (Figure 4.2 (c) the CO_2 laser pulse, and an expansion of the time period where the level of the HgCdTe and PMT signal changes (Figure 4.2 (d)). The PMT signal and the HgCdTe signal were Fourier analyzed; Figure 4.2 (e) shows the spectrum of the PMT signal during the pulse, Figure 4.2 (f) shows the spectrum of the PMT signal after the pulse, Figure 4.2 (g) represents the spectrum of the HgCdTe signal); for the discussion of these FFT-data, see chapter 4.3.4.

* 500 W/3 mm is shown in Figure 4.3 as an example of the PMT signal from a conduction limited weld. This figure includes an overview of the whole sampling period (Figure 4.3 (a)). Since this run includes only a few oscillations during and no oscillations after the CO_2 laser pulse plots of the PMT signal's behavior during and after the pulse are not included. The time difference between the change of the HgCdTe and the PMT signal is shown in Figure 4.3 (b). FFT spectra of this run were created but they revealed an amplitude of the PMT and HgCdTe signal which is significantly lower than for the previous case (about two orders of magnitude); for this reason, these plots are not included.

* 2500W/1 mm is shown in Figure 4.4 as an example of the PMT signal from the lower surface. The selection of the figures follows the same criteria as in the case of Figure 4.2.

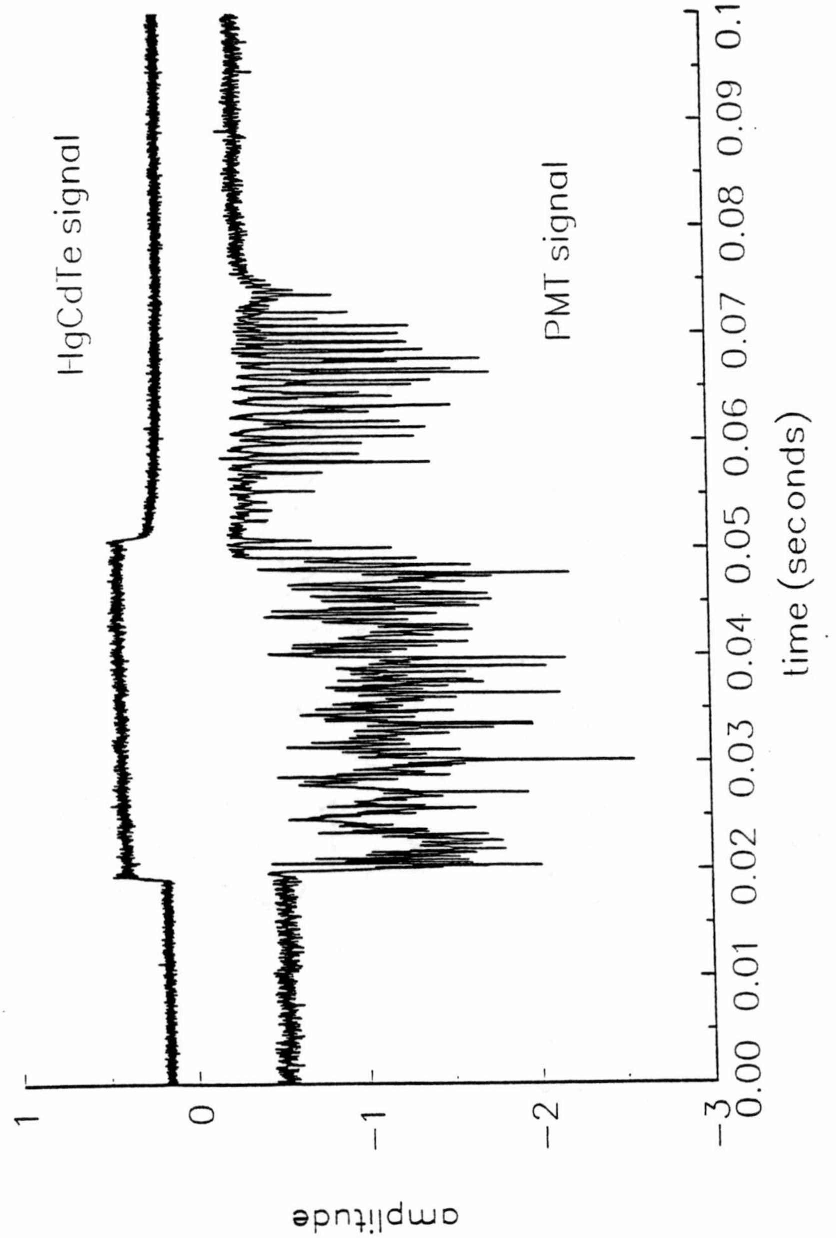

Figure 4.2 (a) HgCdTe and PMT signal for 1500 W/1 mm, overview. The general behavior of the PMT signal before, during and after the CO_2 laser pulse for a deep penetration weld is shown. Oscillations can be identified during and after the pulse.

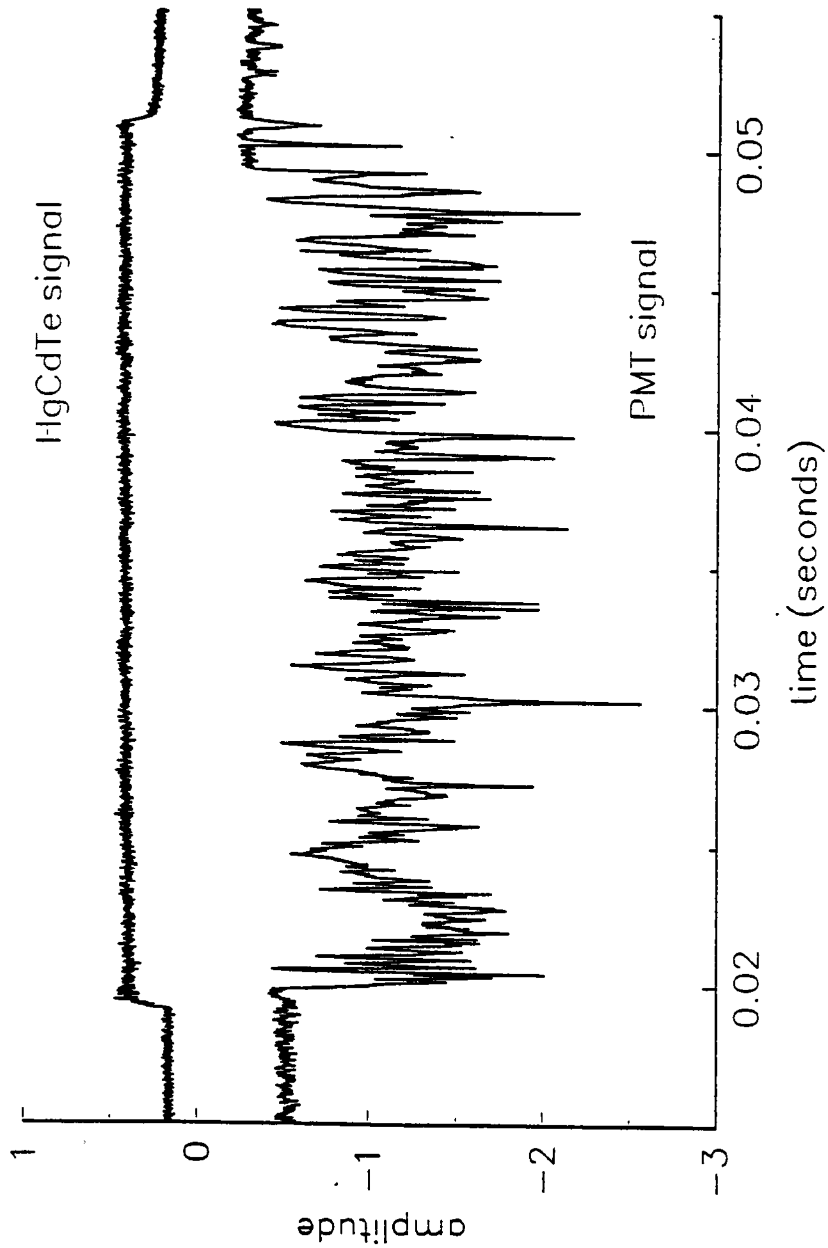

Figure 4.2 (b) HgCdTe and PMT signal for 1500 W/1 mm, during the CO_2 laser pulse. This figure shows an expansion of the behavior of both signals during the CO_2 laser pulse.

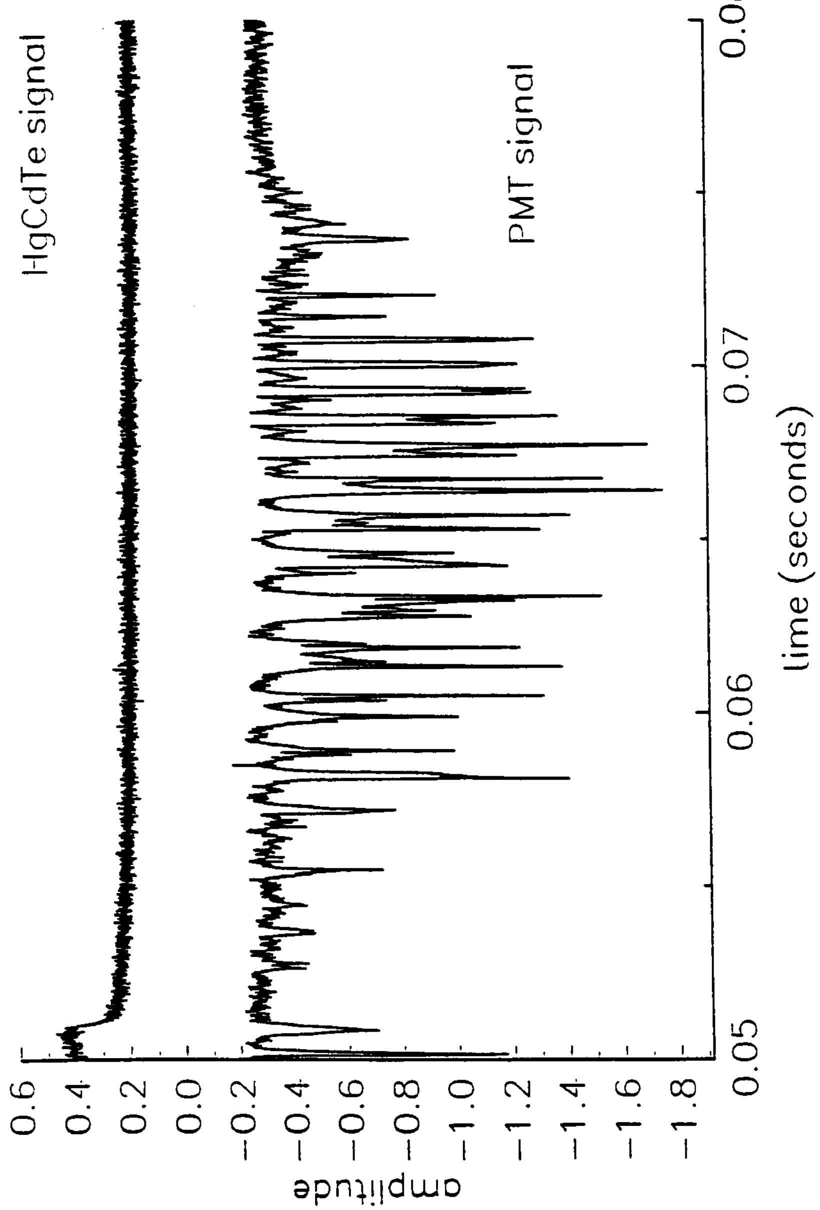

Figure 4.2 (c) HgCdTe and PMT signal for 1500 W/1 mm, after the CO_2 laser pulse. The oscillations of the PMT signal during this expanded period after the CO_2 laser pulse ends are clearly visible.

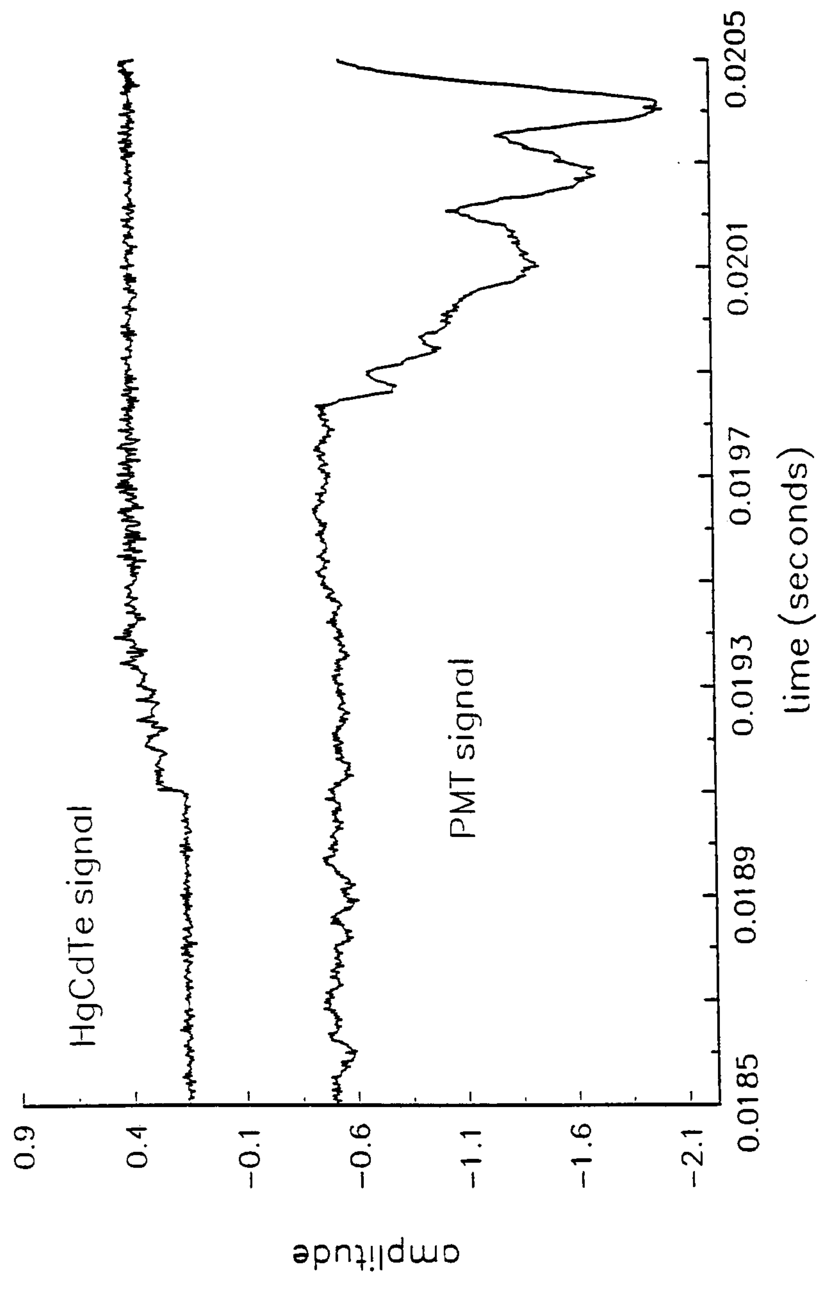

Figure 4.2 (d) HgCdTe and PMT signal for 1500 W/1 mm, phase transition time. The time difference between the changes of the HgCdTe and PMT signal is expanded. This time was called "phase transition time".

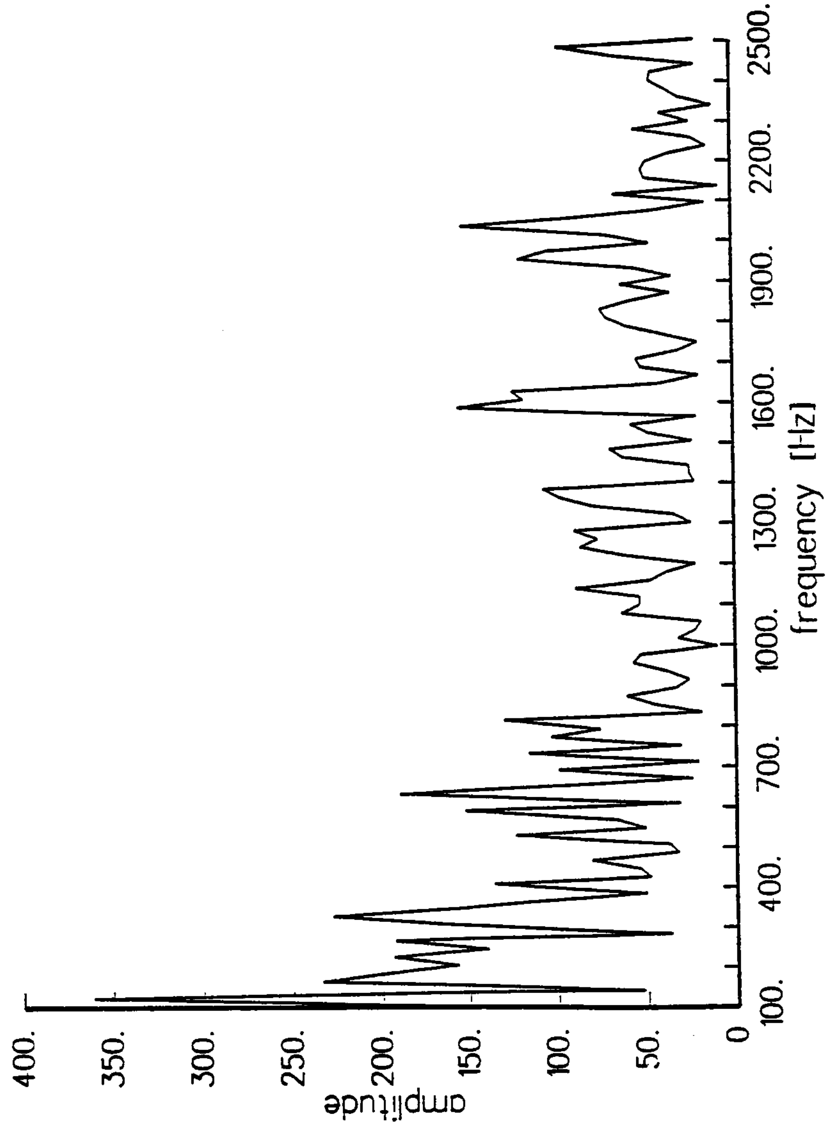

Figure 4.2 (e) Spectrum of PMT signal during the pulse for 1500 W/1 mm. The PMT signal during the CO_2 laser pulse was Fourier analyzed; it can be seen in the power spectrum that low frequencies are represented strongly.

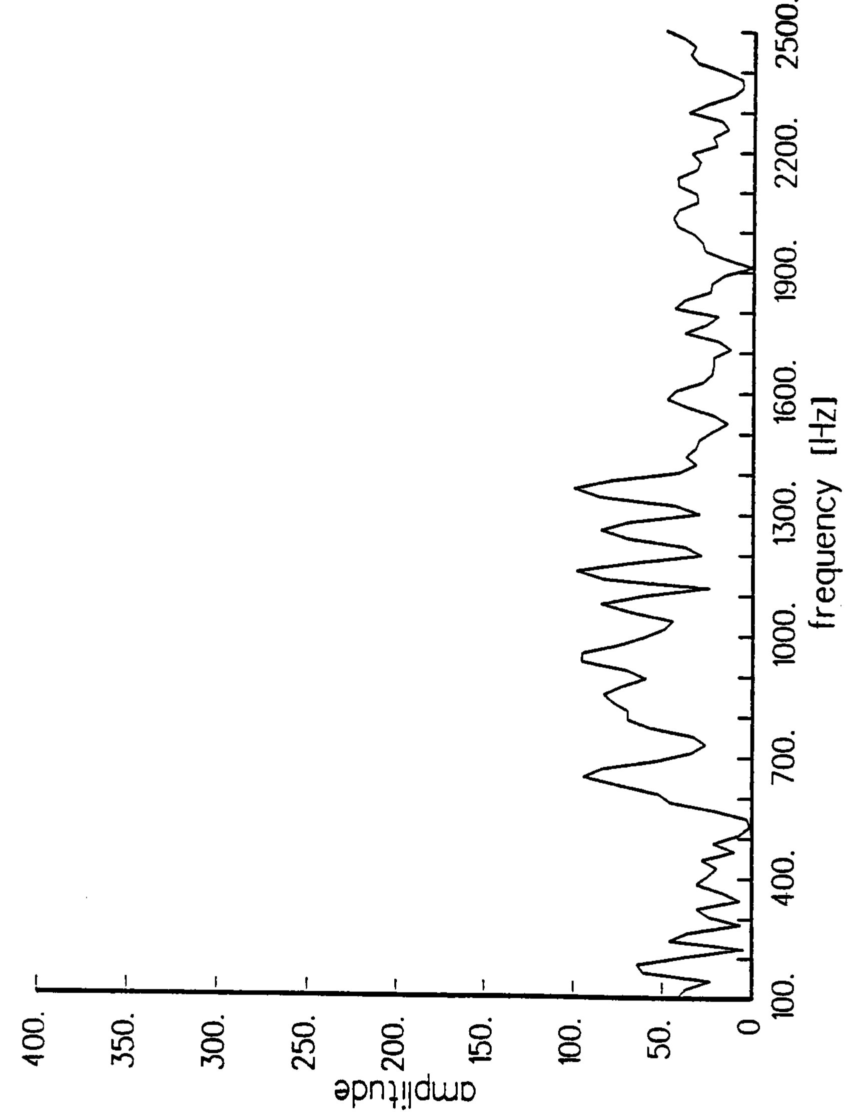

Figure 4.2 (f) Spectrum of PMT signal after the pulse for 1500 W/1 mm. The PMT signal after the CO_2 laser pulse was Fourier analyzed; frequencies between 600 Hz and 1400 Hz are represented strongly.

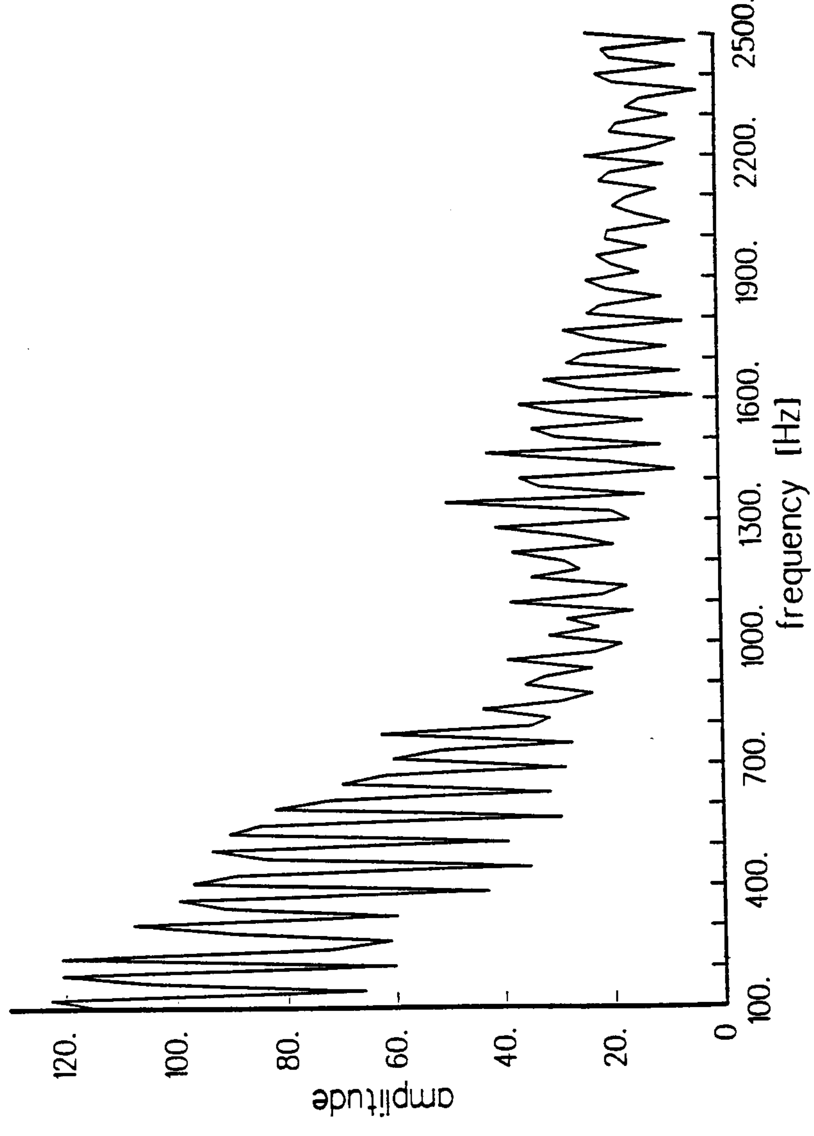

Figure 4.2 (g) Spectrum of HgCdTe signal for 1500 W/1 mm. The HgCdTe signal was Fourier analyzed. The power distribution decreases strongly between 100 Hz and 1000 Hz; for higher frequencies, the power decreases more gradually.

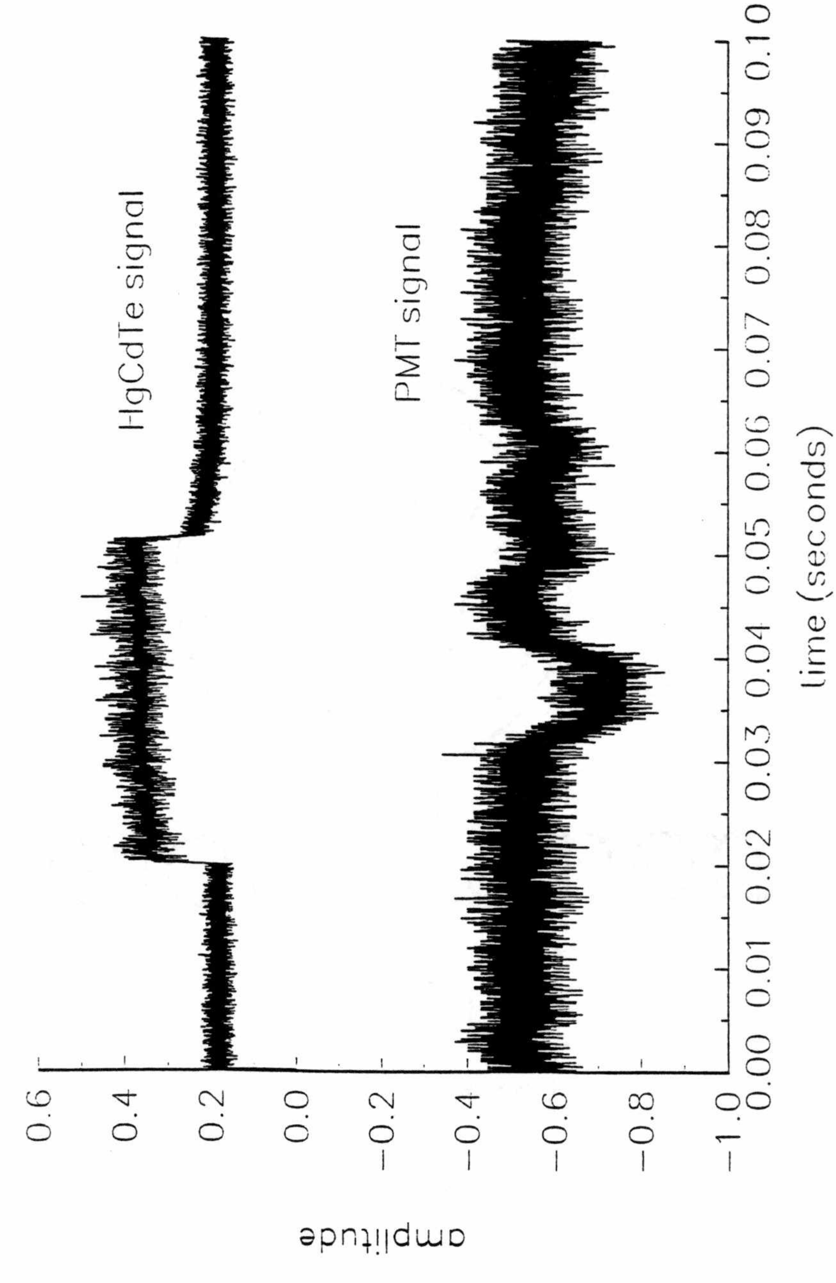

Figure 4.3 (a) HgCdTe and PMT signal for 500 W/3 mm, overview. The general behavior of the PMT signal before, during and after the CO_2 laser pulse for a conduction limited weld is shown. Few oscillations can be identified during and after the pulse.

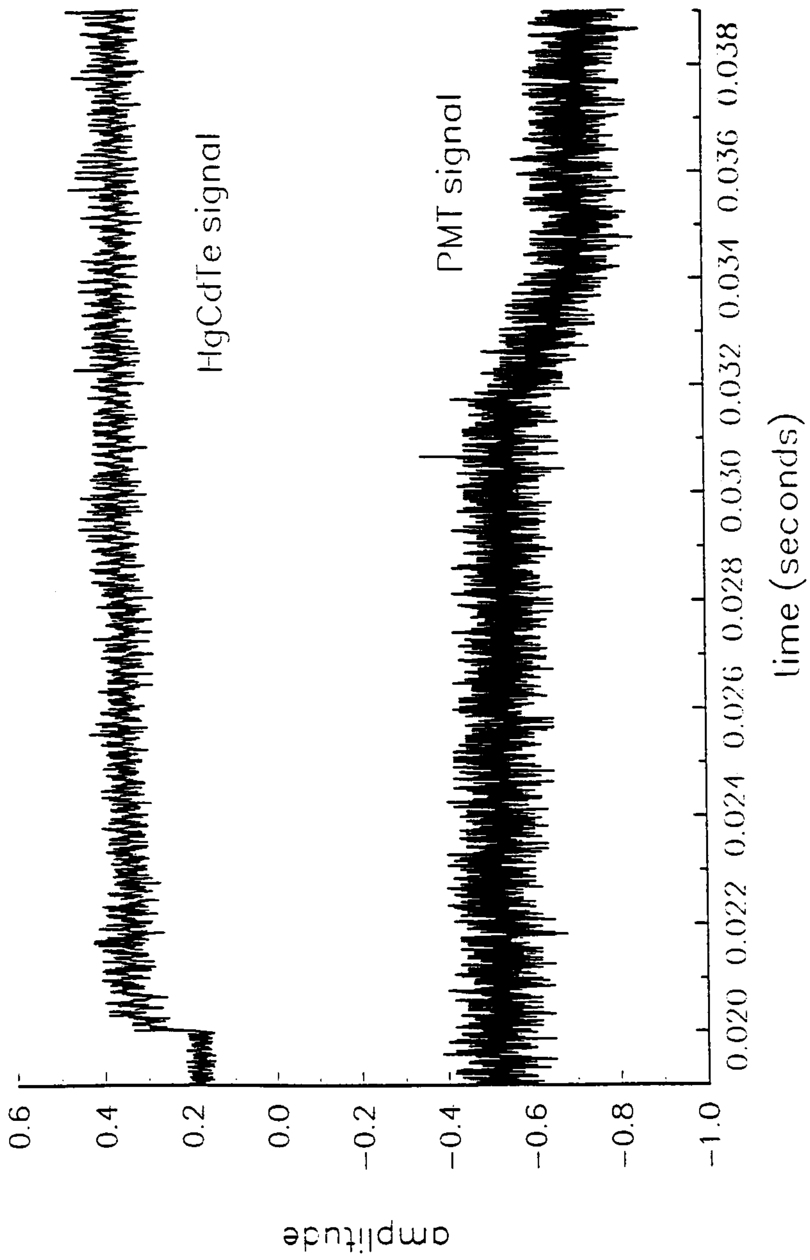

Figure 4.3 (b) HgCdTe and PMT signal for 500 W/3 mm, phase transition time. The time difference between the changes of the HgCdTe and PMT signal is expanded.

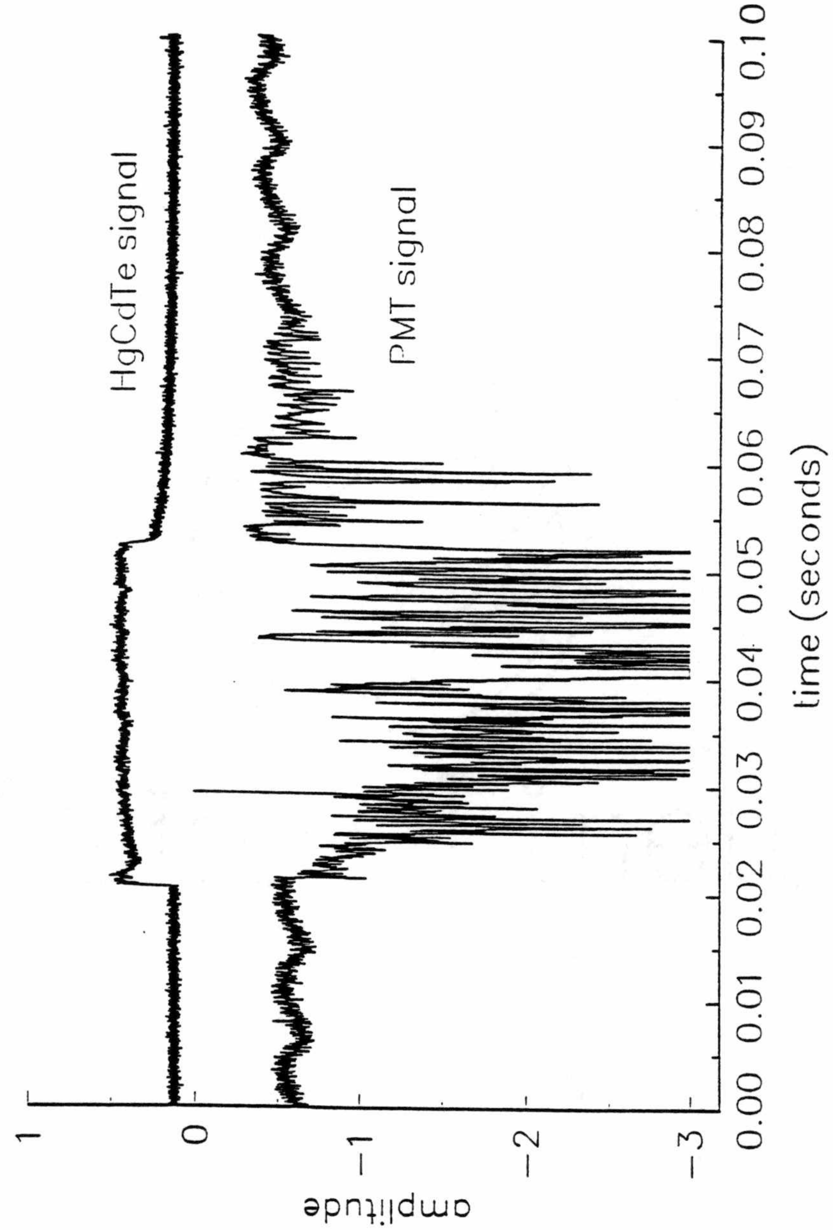

Figure 4.4 (a) HgCdTe and PMT signal for 2500 W/1 mm, PMT data taken from lower surface, overview. The general behavior of the PMT signal for monitoring the lower sample surface is shown. Oscillations can be identified during and after the pulse.

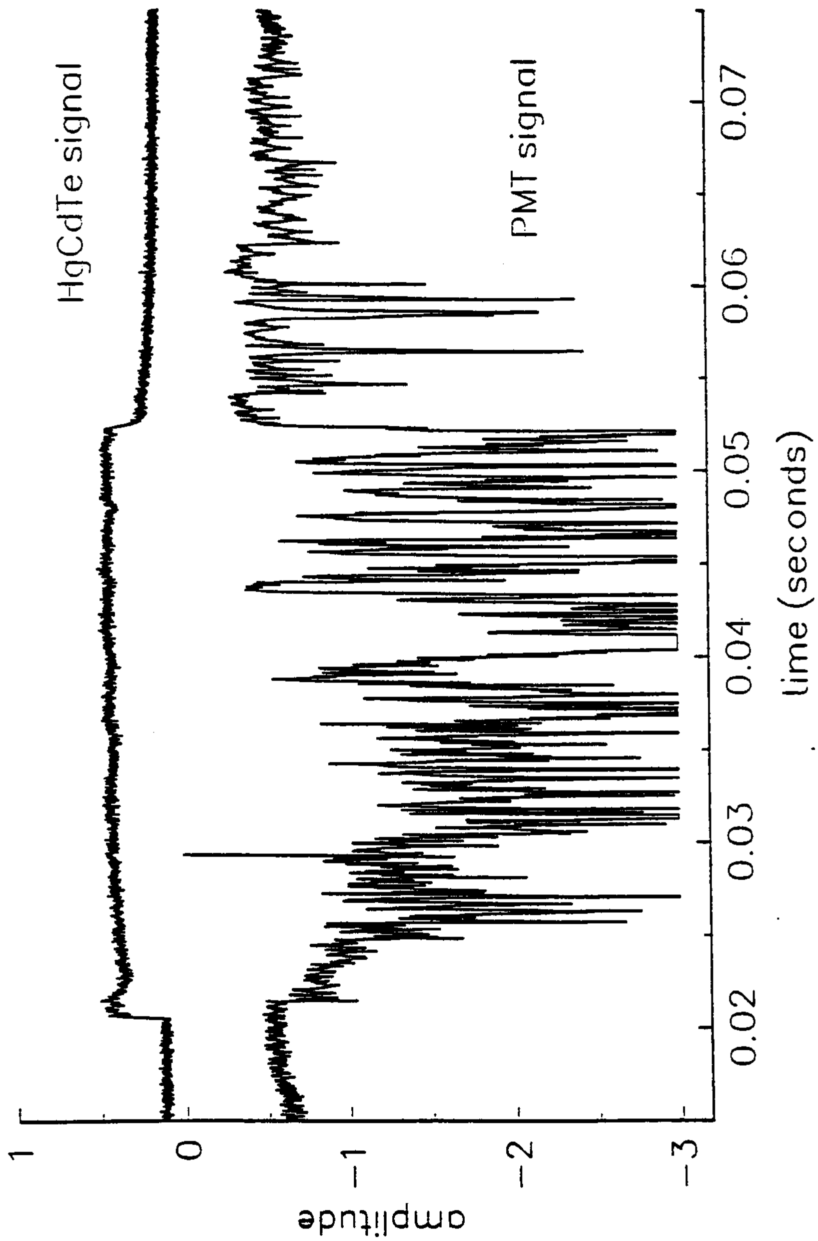

Figure 4.4 (b) HgCdTe and PMT signal for 2500 W/1 mm, PMT data taken from lower surface, during and after the CO_2 laser pulse. This figure shows an expansion of the behavior of the PMT signal.

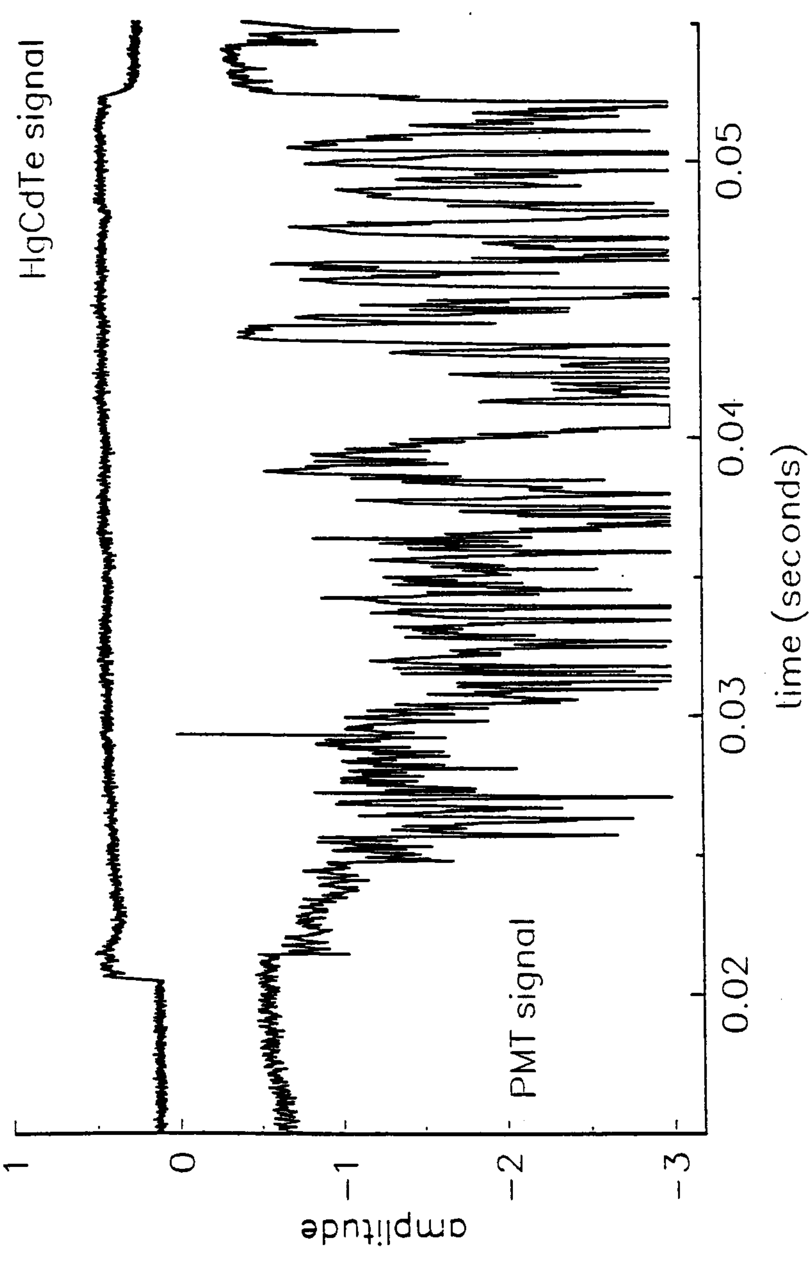

Figure 4.4 (c) HgCdTe and PMT signal for 2500 W/1 mm, PMT data taken from lower surface, during the CO_2 laser pulse. This figure shows an expansion of the behavior of the PMT signal.

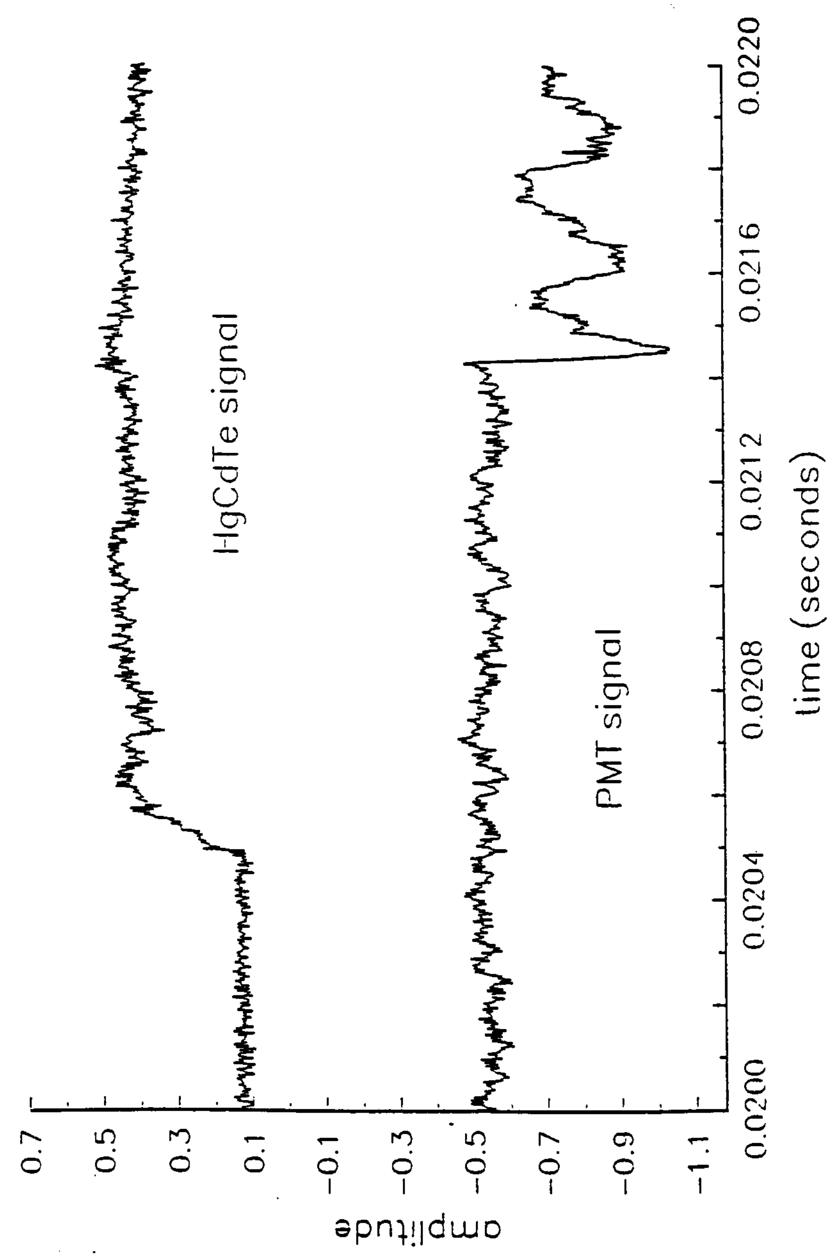

Figure 4.4 (d) HgCdTe and PMT signal for 2500 W/1 mm, PMT data taken from lower surface, penetration time. The time difference between the changes of the HgCdTe and PMT signal is expanded. This time was called "penetration time".

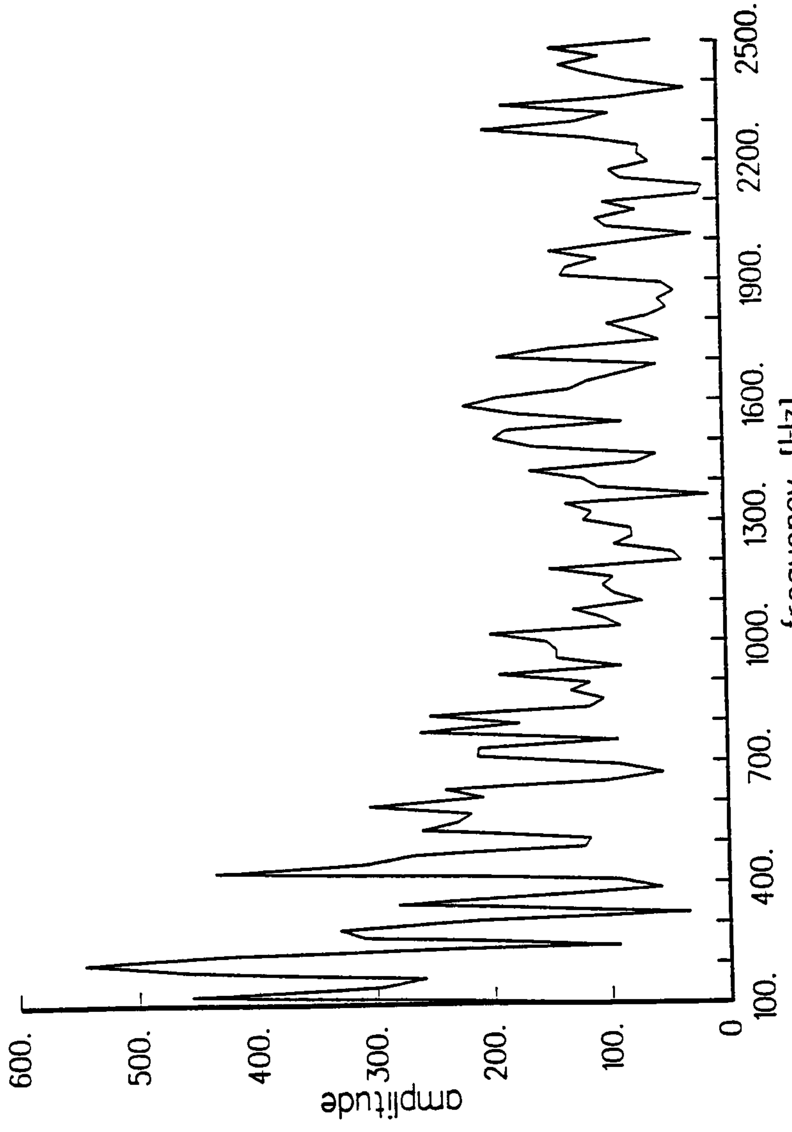

Figure 4.4 (e) Spectrum of PMT signal from lower surface during the pulse for 2500 W/1 mm. The PMT signal during the CO_2 laser pulse was Fourier analyzed; the power spectrum shows low frequencies represented strongly.

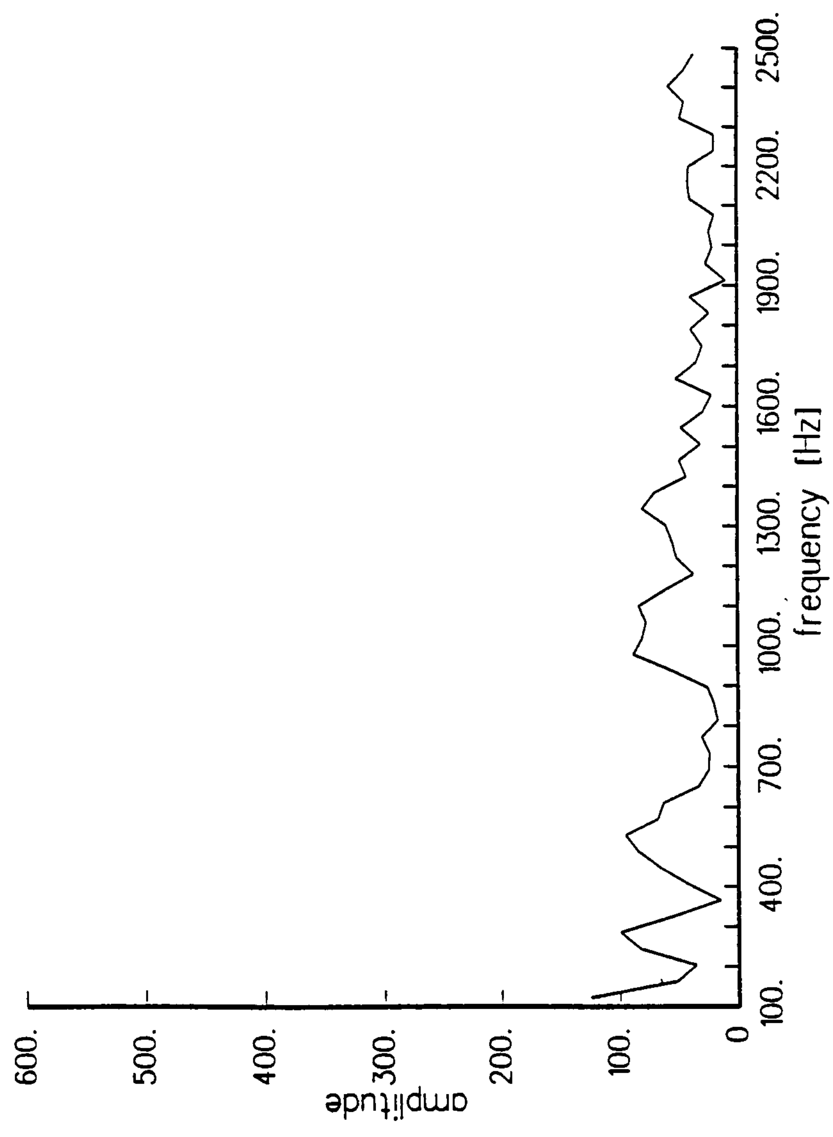

Figure 4.4 (f) Spectrum of PMT signal from lower surface after the pulse for 2500 W/1 mm. The PMT signal after the CO_2 laser pulse was Fourier analyzed; no frequency domain dominates strongly.

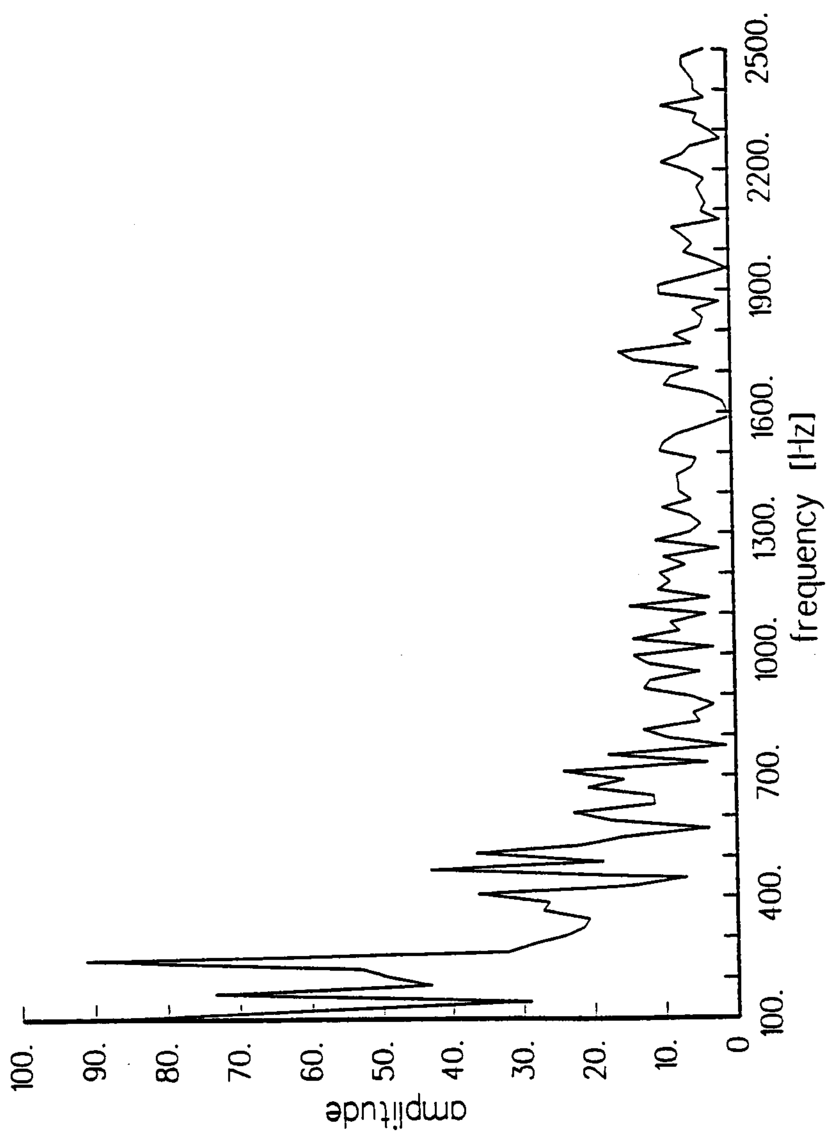

Figure 4.4 (g) Spectrum of HgCdTe signal for 2500 W/1 mm, PMT signal taken from lower surface. A Fourier analysis of the HgCdTe signal shows a strong decrease of the power distribution between 100 Hz and 1000 Hz; for higher frequencies, the power decreases more gradually.

4.3 Upper sample surface

4.3.1 Segment I - Transition period

As described, the PMT signal shows a transition period in the beginning of the CO_2 laser pulse with either an increase or a decrease before it reaches its ground level during the laser pulse. The increase could be caused by one of the following effects:

* An additional high-intensity light source (e. g. plasma) forms above the weld region and emits light which passes through the interference filter. To investigate this possibility, "blind runs" without the Argon laser illumination were performed. Since for both sides of the sample these runs showed that no signal was received by the PMT during the CO_2 laser pulse, this possibility must be excluded.
* The molten metal radiates at 514.5 nm. This cause can be rejected on the same grounds as the previous case.
* The reflectivity from the molten metal is higher than from a solid metal surface. Indeed, it has been shown [8] that the reflectivity of a surface of liquid metal is a strong function of the incident angle. During the formation of the weld pool and the keyhole, the surface of the weld pool changes as described in chapter 2.2. Consequently, the angle of incidence of the Argon laser beam with respect to the surface normal of the weld pool surface will vary during this period. Therefore,

it is possible that the Argon laser beam is incident on the sample surface at an angle at which the reflectivity of the molten metal is higher than the reflectivity of the solid metal.

* The sample surface acts as a concave or a convex reflector. To illustrate this the different beam paths are schematically shown in Figure 4.5. An incident focused Argon laser beam will be reflected from a flat sample surface as shown in Figure 4.5 (a). When this sample is hit by the CO_2 laser beam and its temperature begins to rise, it is conceivable that the material locally expands and forms a "bump" on the sample surface. The same incident beam will then be reflected as shown in Figure 4.5 (b). If a depression with a large radius of curvature is formed on the surface of the weld pool the Argon laser beam will be reflected as shown in Figure 4.5 (c). For the latter two cases, the distance of the focal point from the sample surface is determined by the radius of curvature of the depression. If the PMT is mounted at a distance close to the focal distance of the curved sample surface the intensity of the Argon laser beam received by the PMT will be higher than in case (a).

4.3.1.1 Interpretation of the transition period

By recording the PMT and the HgCdTe signal simultaneously, the time delay of the PMT signal relative to the start of the CO_2 laser pulse can be measured. Since the

(a)

(b)

(c)

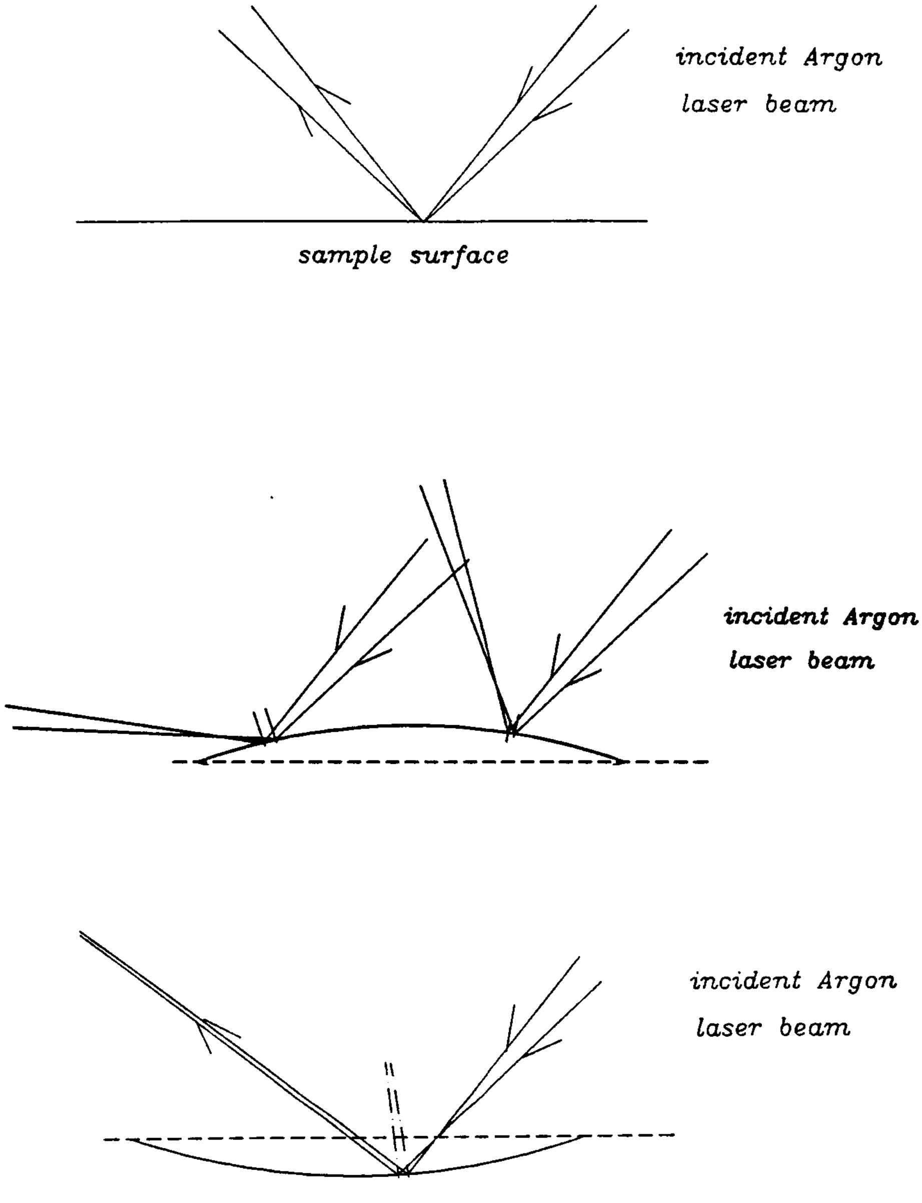

Figure 4.5 Schematic of the path of the Argon laser beam reflected from (a) a flat surface, (b) a convex surface, (c) a concave surface.

sample is not translated in any direction the PMT signal can only change if the surface deforms in the presence of the CO_2 laser beam.

By using the laser reflectometer, the physical processes contributing to this deformation of the surface cannot be specified. It is possible that ablation of the material, sublimation, a solid-liquid phase change followed by a liquid-vapor phase change, or a combination of these processes [8] are involved. The laser reflectometer used in this investigation is capable of detecting temporarily varying structures on the sample surface, but it cannot identify the phases (e. g. solid or liquid) present. The time differences between the PMT and the HgCdTe signal have been extracted and are listed in Table 4.1 and Table 4.2.

Since it is known that a phase transition occurs, "phase transition time" was chosen as the nomenclature to describe the time delay between the CO_2 laser pulse and the change in the level of the PMT signal.

Table 4.1 Phase transition time t_{PT} taken from PMT data (sample thickness 1 mm).

Power [W]	sample thickness [mm]	t_{PT} [μs]
2500	1	80
2000	1	560
1500	1	730
1000	1	10
500	1	200

Table 4.2 Phase transition time t_{PT} taken from PMT data (sample thickness 3 mm).

Power [W]	sample thickness [mm]	t_{PT} [μs]
2500	3	130
2000	3	630
1500	3	300
1000	3	1170
500	3	11800

4.3.2 Segment II - Behavior during the CO_2 laser pulse

Most of the PMT data show oscillations during the welding process for both sample thicknesses. To explain this behavior of the PMT signal, the properties of the CO_2 laser beam have to be considered: For the alignment, the Argon laser beam is aimed at point ***a'*** (Figure 4.6) in a resolidified weld pool. However, the spot welds produced by the CO_2 laser are generally elliptical; since they also rotate, the final position of the weld pool and the keyhole is not predetermined. The center of the keyhole can be created at the point where the Argon laser beam is aimed (Figure 4.6, ***a***), or it can be created next to the focal position of the Argon laser beam (Figure 4.6, ***a'***).

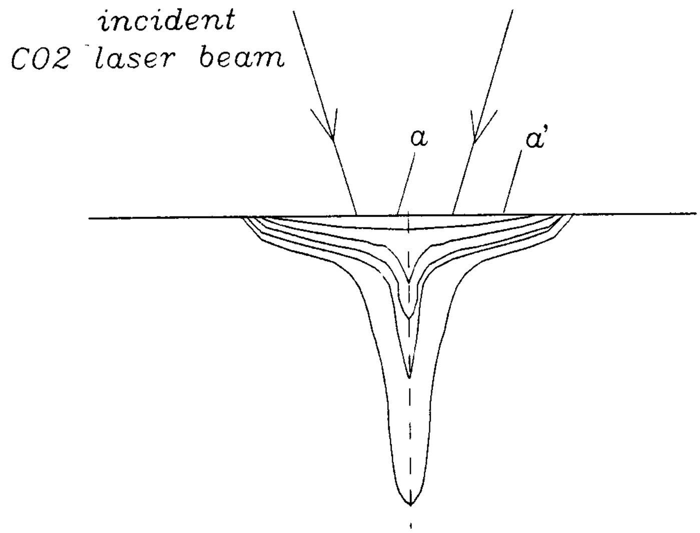

Figure 4.6 Positioning of the focused Argon laser beam relative to the place where the weld region is created and where the keyhole is finally formed. The shape of the liquid-vapor interface during this formation is shown.

If the Argon laser points at the center of the keyhole (Figure 4.6, ***a***), the Argon laser beam will initially be reflected from this surface and when the keyhole itself develops, the Argon laser beam will be "caught" in the keyhole in a similar manner to the operation of a Rayleigh horn. In this case, the PMT signal will show a very short increase followed by a drop to a minimum for the duration of the CO_2 laser pulse. If the Argon laser beam hits the weld region near point ***a'*** (Figure 4.6), it will be reflected from the molten metal. In this case, the reflected beam can be detected by the PMT. The frequency of these waves determines the frequency of oscillations in the PMT signal.

4.3.3 Segment III - Behavior after the CO_2 laser pulse

After the CO_2 laser pulse ends, the keyhole collapses within approximately 0.1 ms. The fluid dynamical processes occurring during the collapse of the keyhole differ for the two sample thicknesses. Qualitatively, the following process takes place.

When the molten material begins to flow back into the cavity (which can be as deep as 3 mm), the level of liquid material in the cavity rises. Its surface must rise to a minimum level before the reflected Argon laser beam is detected again. If the Argon laser beam was caught in the keyhole during the welding process, oscillations can appear in the PMT signal, beginning at a certain time after the end of the CO_2 laser pulse. This time is determined by the velocity of the material at the surface and the depth of the keyhole.

Superimposed on this process is a decrease of the temperature of the liquid metal since the energy source (CO_2 laser) is shut off. If the temperature of the liquid metal decreases below its melting temperature, the material will begin to solidify after some time Δt, estimated as follows: At most, the temperature of the molten metal can be the vaporization temperature $T_v \approx 3000$ K. For the material to solidify, its temperature has to decrease to $T_m \approx 1800$ K. Assuming a maximum temperature gradient with respect to time of 10^5 K/s [12], the typical time scale would be $(T_v - T_m)/(dT/dt) = 1200\ K/(10^5\ K/s) = 12\ ms = \Delta t$. If the collapsing cavity fills in a time shorter than Δt, the molten metal can reach the minimum level in the cavity from which the Argon laser beam can be reflected towards the PMT. Then, the PMT signal will show oscillations which originate from the surface waves on the liquid metal. These oscillations begin some time after the CO_2 laser pulse ends, and have the frequency of the surface waves. The end of these oscillations can be taken as a first estimate of when the temperature of the material approaches the solidification temperature.

4.3.4 FFT spectra

The oscillations which appear in the PMT signal during and after the CO_2 laser pulse are a significant feature of these signals. Since these oscillations appear to have a dominant frequency (Figure 4.2) together with (occasionally) high amplitudes, a Fast Fourier Transformation (FFT) analysis of the PMT signal was made. To ensure that the program was operating properly, the drive current signal which includes the 5 kHz modulation was analyzed. The 5 kHz frequency and its first harmonic were identified. Also, the HgCdTe signal was analyzed and shown to included the 5 kHz modulation.

The limits of the FFT analysis are determined by the sampling rate and the length of the sampling interval, with the Nyquist-criterion used to determine the minimum and maximum reliable frequency. In order to avoid aliasing of a signal, the sampling rate must be at least 2.5 to 3 times as high as the highest frequency of interest. Therefore, for a sampling rate of 3 μs the highest reliable frequency which can be extracted from the corresponding signal is approximately 110 kHz. Hence, for a sampling interval of 30 ms, a period of at the most 10 ms can be reliably identified. This converts into a minimum observable frequency of 100 Hz.

FFT spectra were obtained in cases where the PMT signal contained oscillations during or after the CO_2 laser pulse. The HgCdTe signal was similarly analyzed for these cases.

Generally speaking, the amplitudes of the spectra of oscillations during the CO_2 laser pulse (Figure 4.2 (e)) are much stronger and more irregular than those after the pulse (Figure 4.2 (f)). PMT (Figure 4.2 (g)) and HgCdTe spectra taken from oscillations during the pulse mostly show the same overall tendency. Most power is contained in the low frequency range; the power distribution decreases rapidly from 100 Hz to about 1000 Hz. Increasing in frequency from 1000 Hz, the power level rolls-off more gradually until the noise level is reached at about 2500 Hz. Based on these results, it can be concluded that the sample is not oscillating at its resonant frequency (24 kHz) during the welding process.

The power distribution showed spikes at the frequencies listed in Table 4.3 for a sample thickness of 1 mm and in Table 4.4 for a sample thickness of 3 mm.

Table 4.3 High-power frequency of the PMT signal for a sample thickness of 1 mm

incident power [W]	sample thickness 1 mm	
	frequencies during pulse [Hz]	frequencies after pulse [Hz]
2500	200	350
2000	250	300
1500	200, 350, 1600	600 - 1400
1000	keyhole (no reflections)	300
500	350	200

The resonance frequency determined in Appendix A under the listed assumptions for a cylinder of liquid metal is between 200 Hz and 300 Hz. Since the geometry and the thermophysical constants used (see Appendix C) differ from the real conditions, one can only surmise that the resonance frequency for the weld is a low frequency of a few hundred Hertz. This is consistent with the frequencies found in the FFT spectra of the PMT signals. From this, it can be concluded that the model described in Appendix A is a good approximation.

Table 4.4 High-power frequency of the PMT signal during the pulse for a sample thickness of 3 mm. The PMT signal contained no oscillations after the pulse.

incident power [W]	frequencies during pulse [Hz]
2500	200
2000	250
1500	600 - 1400
1000	keyhole (no reflections)
500	350

It has been shown [15] that the wavelength of the surface waves is approximately 250 μm. Multiplying this number with the dominant frequencies listed in Table 4.3 and Table 4.4, the velocity of the surface waves is found to be 0.05 m/s (frequency of 200 Hz) to 0.4 m/s (frequency of 1600 Hz). These values compare well with reported velocities (0.1 m/s to 1 m/s, [12, 14]).

Using non-dimensional numbers, it is now possible to confirm the existence of waves on the sample surface. In terms of the kinetic energy of the molten metal compared to its potential energy, the Froude number Fr can be calculated. Assuming an average surface wave velocity of 0.2 m/s and a characteristic length (keyhole depth) of 1 mm, $Fr = 4 > 1$, confirming the existence of surface waves.

Additional information which can be obtained from knowing the surface wave velocity is an estimation of the amplitude of the surface waves. Assuming that the surface waves form a sine wave, the velocity of these waves is the derivative of the local position of the waves with respect to time. From this, the amplitude of the surface waves can be estimated as

$$A = \frac{vT}{2\pi} \tag{4.1}$$

where v is the velocity of the surface waves and T is the period of these waves. Assuming a velocity of 0.2 m/s and an according period of 1.25 ms, the amplitude of these waves can be estimated as 40 μm.

4.4 Lower sample surface

4.4.1 Introduction

The behavior of the PMT signal detected from the lower side of the sample surface can be analyzed similarly. However, the time delay between the CO_2 laser pulse and the increase in the PMT signal from the lower surface is interpreted as penetration time of the laser beam. The average penetration velocity can be compared to the velocity of the vaporization front.

Fully penetrated samples were obtained for

* 2500 W for a sample thickness of 3 mm
* 2500 W to 1500 W for a sample thickness of 1 mm.

4.4.2 Segment I - Transition period

The distances of the focal lens and the PMT to the weld pool are the same as for the observations of the upper surface; therefore, the same characteristics of the reflected Argon laser beam can be expected.

When the lower surface opens during the development of the keyhole, the Argon laser beam is "caught" in the keyhole. Like in the case of the upper surface, the PMT signal shows a very short increase during this process followed by a drop to a very low level for the rest of the CO_2 laser pulse. This can be caused by the same effects as described for the upper sample surface. If the Argon laser beam hits at the outer weld region, it will be reflected from the molten metal and is detected by the PMT.

4.4.2.1 Penetration sequence

Since no mechanical deformation is present and the sample is not translated in any direction, the PMT signal can only change when the energy of the CO_2 laser beam has penetrated the sample, causing e. g. a volumetric expansion. The time difference between the beginning of the CO_2 laser pulse and the level change in the PMT signal is then the penetration time of the material.

The penetration time depends on the sample thickness. The penetration times extracted from the PMT signal are listed in Table 4.5 (for a sample thickness of 3 mm) and in Table 4.6 (for a sample thickness of 1 mm).

Table 4.5 Penetration times t_p taken from PMT data for a sample thickness of 3 mm

Power [W]	sample thickness [mm]	penetration time [μs]
2500	3	7740

Table 4.6 Penetration times t_p taken from PMT data for a sample thickness of 1 mm

Power [W]	sample thickness [mm]	penetration time [μs]
2500	1	930
2000	1	3100
1500	1	7400

Most PMT signals show a 120 Hz-cycle before and after the CO_2 laser pulse. This is probably electrical noise. For these runs, the amplitude of the 120 Hz-cycle was taken as the maximum and minimum PMT signal level (forming an envelope) before the CO_2 laser pulse. The penetration time was taken as the time when the PMT signal first assumed values outside this envelope.

Dividing the sample thicknesses by the penetration times the following average penetration velocities can be calculated (Table 4.7). These experimentally determined velocities values are in the range as reported in the literature [12].

Table 4.7 Penetration velocities as calculated on the basis of the penetration times as listed in Table 4.5 and Table 4.6.

Power [W]	sample thickness [mm]	penetration velocity [m/s]
2500	1	1.08
2000	1	0.32
1500	1	0.14
2500	3	0.39

4.4.3 Segment II - Behavior during the CO_2 laser pulse

The PMT signals show oscillations during and after the welding process. Remembering that the lower surface opens for these runs the PMT signal can be explained in the same way as in the case of the upper surface where it was shown that the PMT signal depends on the relative position of the Argon laser beam to the point of penetration.

4.4.4 Segment III - Behavior after the CO2 laser pulse

The results obtained by applying the laser reflectometer technique can be used to suggest a possible explanation for the observed concave shape of the resolidified lower surface of 3 mm thick samples.

Considering an average velocity of the molten material of 0.2 m/s a dimensional analysis reveals a typical time scale to fill a 3 mm deep keyhole of 3 mm/(0.2 m/s) = 15 ms. This time scale matches the time scale for the resolidification of the molten metal (12 ms). Thus, it is possible that the molten material which is mainly located at the upper surface resolidifies before it reaches the lower surface. This could explain that the resolidified surface of the penetration point is concave for a 3 mm thick sample.

4.4.5 FFT spectra

As for the signals of the upper surface, FFT spectra were made from cases where the PMT signal contained oscillations during or after the CO_2 laser pulse; however, no dominant frequency could be identified in the FFT analysis.

Generally speaking, the amplitudes of the spectra of oscillations during the CO_2 laser pulse are noisier and have a higher amplitude than those from oscillations after the pulse. In all spectra, the power is distributed over a wide frequency band. No correlation between the PMT spectra taken from oscillations during the pulse and the according HgCdTe spectra is obvious.

5 Conclusions and Recommendations

A diagnostic technique for monitoring the surface of the weld pool during and after the welding process was successfully developed and demonstrated. The diagnostic technique enables the user to collect the following information:

* By showing that there are different signatures for a conduction limited weld and a deep penetration weld, the diagnostic technique allows the user to distinguish between the two welding conditions.

* For the first time, the frequency of the waves on the weld pool surface have been measured. Their velocity is calculated as 0.05 m/s to 0.4 m/s which is in the lower range of velocities reported in the literature.

* The amplitude of the waves on the weld pool surface is estimated as 40 μm.

* During the CO_2 laser pulse, oscillations with occasionally high amplitudes could be identified in the PMT signal. An FFT spectrum revealed that the strongest frequencies exist around 200 Hz to 350 Hz. This agrees well with an estimation of the resonant frequency of a cylinder of liquid metal held in a sheet of solid metal.

* Oscillations after the end of the weld pulse are probably caused by the motion of the molten metal flowing back into the cavity. These oscillations appear in the PMT signal within a time scale determined by the velocity of the surface waves closing the keyhole and the depth of the keyhole.

* The time required for the lower surface to melt (i. e. the penetration time) was measured as less than eight milliseconds for the sample thicknesses and power levels investigated here.

Recommendations

The laser reflectometer technique provides useful information with very high spatial and temporal accuracy. An application of this technique would be to measure the radial velocity distribution of the liquid material on the surface of the weld pool. The data could also be used to estimate the magnitude of the surface tension gradients. In addition, they could be used to relate the velocity of the surface waves and their amplitude to the depth of the liquid weld pool. By comparing this information with existing numerical models which relate the depth of a fluid to the waves appearing on its surface, one can get a better understanding of the relationship between surface tension and the behavior of a liquid pool.

References

References

1 Arata, Y.; 1972 Some fundamental properties of high power laser beam as a heat source (report I); Plasma, Electron, and Laser Beam Technology, publ. by American Society of Metals, Metals Park, OH 44073

2 Arata, Y.; Maruo, H.; Miyamoto, T.; Takeuchi, S.; 1976 Dynamic Behavior of Laser Welding and Cutting; 7th international conference electron and ion beam science and technology

3 Arata, Y.; Miyamoto, T.; 1978 Laser Welding; Technocrat, 11.5, pp. 33 - 42

4 Arata, Y.; 1981 Basic phenomena in high energy-density beam welding and cutting, SPIE Vol. 312 First European conference on Cineradiography with photons or particles

5 Arata, Y.; Maruo, H.; Miyamoto, T.; Inoue, Y.; 1983 Beam hole behavior during laser beam welding; LIA ICALEO 1983, 38, pp. 59 - 66

6 Avallone, E.; Baumeister III, T.; 1987 Mark's standard handbook for mechanical engineers; ninth edition; McGraw-Hill

7 Dowden, J.; Kapadia, P.; Postacioglu, N.; 1989 An analysis of the laser-plasma interaction in laser keyhole welding, J. of Phys. D: Appl. Phys., 22, pp. 741 - 749

8 Duley, W.; 1976 CO_2-lasers, effects and applications; Academic Press, New York

9 Iida, T.; Guthrie, R.; The physical properties of liquid metals, 1988, Clarendon Press, Oxford, UK

10 Kahlen, F.-J.; 1992 Diagnostics for liquid rocket propulsion instability measurements, Diplomarbeit at the Rheinisch-Westfälisch Technische Hochschule Aachen

11 Kroos, J.; Gratzke, U.; Vicanek, M.; Simon, G.; 1993 Dynamic behaviour of the keyhole in laser welding; J. of Phys. D: Appl. Phys., 26, pp. 481 - 486

12 Miyamoto, I.; Maruo, H; Arata, Y.; 1986, Beam Absorption Mechanism in Laser Welding; SPIE Vol. 668 Laser Processing: Fundamentals, Applications, and Systems Engineering, pp. 11 - 18

13 Renz, U.; 1991 Grundlagen der Wärmeübertragung; lecture notes from graduate course "Wärmeübertragung", Lehrstuhl für Wärmeübertragung und Klimatechnik, Rheinisch-Westfälisch Technische Hochschule Aachen

14 Sakout, A.; Dard, J.; Laurent, M.; 1987 Une Modelisation des Champs de Temperature en soudage Laser CO_2; Journal de Physique, Colloquesv 48 No. C7, pp. 163 - 166

15 Semak, V.; Kahlen, F.-J.; McCay, T. D.; McCay, M. H.; 1993 Laser keyhole study using laser reflectometer and high speed photography; LIA ICALEO 1993, presentation

16 Swift-Hook, D.; Gick, A.; 1973 Penetration welding with lasers; Welding Journal, 52, Research Supplement, pp. 492s - 499s

Appendices

Appendix A

Resonance frequency of a cylinder of liquid material

Suppose that a cylinder of material has been molten by the CO_2 laser beam with the geometry of the problem as shown in Figure 1. Assuming that the surface of the fluid remains flat the condition at rest is that the molten material must be held in place by a force acting along the liquid-solid interface:

$$mg = 2\pi r t \tau \quad \textbf{(A1)}$$

where m is the mass of the liquid material, g is the gravitational constant, r and t are the radius and the height of the cylinder, respectively, and τ represents the shear stress along the liquid-solid interface.

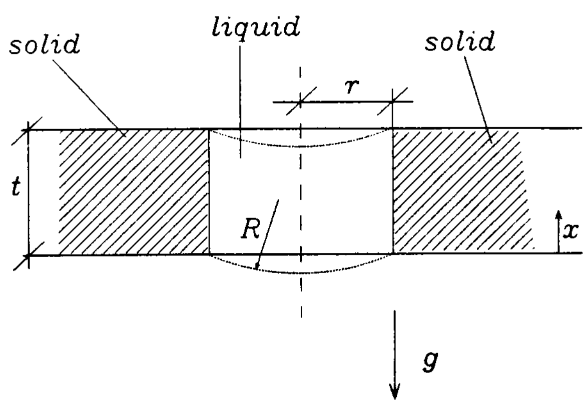

Figure A1 Cylinder of liquid material surrounded by a sheet of solid material. The dotted lines show the displacement of the free surface from the equilibrium position.

If the liquid is moved out of the equilibrium position by an external force which is removed suddenly afterwards a force balance reveals

$$m\ddot{x} = -mg + 2\pi r t \tau + 2\frac{\gamma}{R}S \qquad \textbf{(A2)}$$

where S is the area of the free surface of the liquid and R is its radius of curvature, γ is the coefficient of surface tension, x is displacement of the free surface from its equilibrium position at the center of the displacement; it is assumed that the radius of curvature on both free surfaces are equal. The area S can be calculated by the equation $S = 2\pi Rh$, where h is the displacement of the free surface from its equilibrium position at the center of the displacement. In terms of the coordinates used in Figure 1 it can be seen that $h = -x$.

Now, with a few simple manipulations and by using (1) and $m = \pi r^2 t\rho$, (2) can be changed into

$$\ddot{x}+4\frac{\gamma}{r^2 t\rho}x=0 \qquad \textbf{(A3)}$$

where ρ is the density of the liquid material. From this equation, the resonance frequency of the liquid material can be calculated as

$$f_{res}=\frac{1}{2\pi}\sqrt{4\frac{\gamma}{r^2 t\rho}} \qquad \textbf{(A4)}$$

This equation can be used for a first estimate of the resonant frequency of a fully penetrated spot weld without a keyhole. Using the values as summarized in Appendix ? and a radius $r = 0.5$ mm the resonant frequency for a 1 mm thick sample is calculated as approximately 300 Hz, for a 3 mm thick sample the resonant frequency would be about 170 Hz.

Appendix B

List of equipment

Equipment for Argon beam delivery and detection

1 Photomultiplier Tube (PMT) Hamamatsu R212

1 High Voltage Power Supply Power Designs, Inc. Model 3K10B

1 Neutral Density Filter ∅ 2.54 cm, 4.0, Oriel

1 Neutral Density Filter ∅ 2.54 cm, 1.0, Oriel

1 Interference Filter 514.5 nm (Bandwidth 10 nm)

1 Lens ∅ 2.54 cm, focal length 10 cm

1 resistor 50 kΩ

Equipment for CO_2 laser beam detection and calibration

1 ZnSe Beam Splitter ∅ 5.08 cm, Laser Power Optics

1 ZnSe Lens, ∅ 2.54 cm, focal length 7.5 cm

1 ZnSe Window, broken piece

1 HgCdTe detector

1 Scientech 390 watercooled Calorimeter, Model No. 39-0201

Laser related equipment

1 Rofin-Sinar CO_2-laser RS3000 (max. 2500 W)

1 Workstation with beam delivery optics (45° flat mirror, off-axis parabolic mirror with focal length 150 mm)

1 Lexan 95 Argon laser (max. 3 W)

Miscellaneous

2 PC's 486

mounting equipment (mirrors, post holders, bolts, ...)

List of used software

"WORKBENCH PC 2.0", Strawberry Tree Incorporated

"Axum 2.0" by TRIMETRIX. Inc.

"Jim's Plot Program" v7.0

Appendix C

Properties of Iron and Stainless Steel SS 304

This Appendix summarizes numerical values of thermophysical and mechanical material properties of Stainless Steel SS 304 and Iron for temperatures of 1000 K or higher. Wherever possible, values for SS 304 were used for computations.

Stainless Steel SS 304

Property	Value	Reference
heat capacity c_p [J/(kg*K)]	620, 980	8, 16
thermal conductivity k [W/(m*K)]	24	8, 16

Iron

Property	Value	Reference
surface tension γ [N/m]	1.8	11
density ρ [kg/m^3]	7000	11
thermal diffussivity $\varkappa$ [m^2/s]	$8.6 * 10^{-6}$	11
heat capacity c_p [J/(kg*K)]	750	11
latent heat of fusion [J/kg]	$272 * 10^3$	9
latent heat of vaporization L_v [J/kg]	$6.3 * 10^6$	11
thermal conductivity k [W/(m*K)]	40 - 50	8, 9, 13
melting Temperature T_m [K]	1800	11
vaporization Temperature T_v [K]	3000	11
Young's modulus [N/m^2]	$193*10^9$	6
viscosity μ [mPas]	4 - 6	9

Appendix D

CNC program FJK.P

```
G91            ;move relative to present position
G71            ;use metric units
M85            ;PWM Bypass OFF
M86            ;Pulse enable OFF
M90            ;Turn shield gas flow on
M94            ;Prepulse for triggering and warm up
G4 F15.0       ;turn this prepulse on for 15 seconds
M84            ;end prepulse
G4 F0.25       ;Time delay of 0.25 seconds
(CLS,SHOP)     ;call subroutine "open shutter"
M94            ;Discharge on for WELD PULSE
G4 F0.05       ;Turn weld pulse on for 0.05 seconds *** see NOTE ***
M84            ;Discharge off for END WELD PULSE
(CLS,SHUT)     ;call subroutine "close shutter"
M80            ;Turn shield gas flow off
M2             ;End of Program
```

```
(DFS,SHOP          ;define subroutine "open shutter"
M98
G4 F0.2
M88
)
(DFS,SHUT          ;define subroutine "close shutter"
M99
G4 F0.5
M89
)
```

NOTE:

The CNC timing is not accurate below 0.1 seconds. A command to turn the weld pulse on for 50 milliseconds will repeatedly result in a CO_2-laser pulse of 30 milliseconds $\pm$ 2 milliseconds.

VITA

Franz-Josef Kahlen was born in Eschweiler, Germany on December 13, 1965. He entered the Rheinisch-Westfälisch Technische Hochschule in Aachen, Germany and graduated as Diplom-Ingenieur in September 1992. Franz-Josef Kahlen served as a member of the local "Kreistag" (comparable to county council) in the "Kreis Aachen"/Germany from 1989 to 1992. From November 1991 to May 1992, he worked at The University of Colorado at Boulder as Research Associate for the thesis required for his study in Germany. In January 1993, he entered The University of Tennessee Space Institute in Tullahoma, TN and worked at the Center for Laser Applications as a Research Assistant. He graduated in May 1994.